Distribution Agreement

In presenting this thesis or dissertation as a partial fulfillment of the requirements for an advanced degree from Emory University, I hereby grant to Emory University and its agents the non-exclusive license to archive, make accessible, and display my thesis or dissertation in whole or in part in all forms of media, now or hereafter known, including display on the world wide web. I understand that I may select some access restrictions as part of the online submission of this thesis or dissertation. I retain all ownership rights to the copyright of the thesis or dissertation. I also retain the right to use in future works (such as articles or books) all or part of this thesis or dissertation

Signature:

_____ _____

Aidan Mouat Date

Synthesis and Characterization of the Metal Complexes of [N(*o*-PhNHC(O)Me$_3$]: A Tripodal, Triamidate Ligand Platform

By

Aidan Mouat
Master of Science

Chemistry

_____
Dr. Cora MacBeth
Advisor

_____
Dr. Karl Hagen
Committee Member

_____
Dr. Craig Hill
Committee Member

Accepted:

_____
Lisa A. Tedesco, Ph. D.
Dean of the Graduate School

_____
Date

Synthesis and Characterization of the Metal Complexes of [N(*o*-PhNHC(O)Me$_3$]: A Tripodal, Triamidate Ligand Platform

By

Aidan Mouat

Advisor: Cora E. MacBeth, Ph. D.

An abstract of
a thesis submitted to the Faculty of the Graduate School of Emory University
in partial fulfillment of the requirements for the degree of
Master of Science
in Chemistry

2009

Abstract

Synthesis and Characterization of the Metal Complexes of [N(*o*-PhNHC(O)Me$_3$]: A Tripodal, Triamidate Ligand Platform

By

Aidan Mouat

This thesis reports the synthesis and characterization of a novel tripodal, triamidate ligand [N(*o*-PhNHC(O)Me)$_3$] based on a generic [N(*o*-PhNCH(O)R)$_3$] platform, where R is a series of substituents varying in both steric bulk and electron-donating or –withdrawing ability. The cobalt(II), nickel(II), and zinc(II) metal complexes K[CoN(*o*-PhNC(O)Me)$_3$], K[NiN(*o*-PhNC(O)Me)$_3$], and K[ZnN(*o*-PhNC(O)Me)$_3$] of the R = Me ligand have also been synthesized. These complexes have been characterized using NMR, FTIR, HRMS(ESI), and UV-Vis spectroscopy. They adopt a trigonal monopyramidal geometry which is consistent with other metal complexes of the ligand platform. Spectroscopic data indicate that the complexes are most likely forming in an alternate geometry to the anticipated C_3-symmetric species, occuring either as a C_s-symmetric, mixed donor amidate binding through the O-donor of one of the ligand "arm" and the N-donor of the other two, or as a C_2-symmetric dimer, the model for which has been observed in other complexes of the ligand platform. No X-ray structures of the complexes are available at present, so this geometry remains unverified.

Synthesis and Characterization of the Metal Complexes of [N(*o*-PhNHC(O)Me$_3$]: A Tripodal, Triamidate Ligand Platform

By

Aidan Mouat

Advisor: Cora E. MacBeth, Ph. D.

A thesis submitted to the Faculty of the Graduate School of Emory University
in partial fulfillment of the requirements for the degree of
Master of Science
in Chemistry

2009

Table of Contents

List of Figures

List of Tables

1. Introduction

Tripodal, tetraamine ligand platforms with the general structure presented in Figure 1 have been widely studied because of their many applications in inorganic chemistry. The basic structure of these ligands consists of an apical, tertiary amine with three 'arms' composed of a hydrocarbon backbone and ending in a terminal N-donor atom group. A good example of a basic tripodal tetraamine moiety is that of tris(2-aminoethyl)amine (tren, Figure 2) in which the carbon backbone of each arm is an ethylene unit and the terminal N-donor atoms are simple primary amines. The range of chemistry this structural group offers is due to the variability of its steric and electronic features. These can be easily altered in one of two ways: first, by changing the nature of the backbone of each arm (examples include various lengths of hydrocarbon chains or the addition of heteroatoms to change the electronic character of the backbone); and second, by changing the nature of the terminal and apical donor atom units, either by incorporating a new N-donor functionality (such as the amidates discussed later) or by changing the terminal or apical group to a new donor atom, such as O, S, or P.[1]

Figure 1: Generic tripodal tetraamine

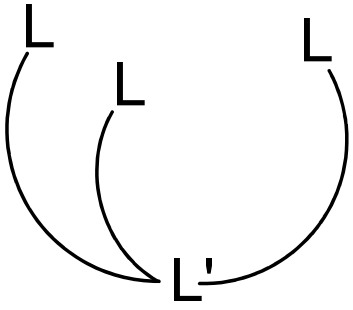

Figure 2: Tris(2-aminoethyl)amine (tren)

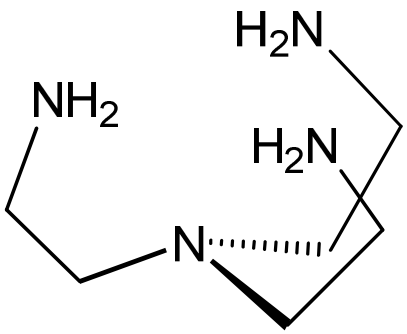

A class of compounds derived from the basic tetraamine precursors that has received wide discussion in the literature is that of "tripodal, trianionic triamidoamines"[2]. Shrock et al. have produced a great deal of work with ligand systems of the general formula $[(RNCH2CH2)_3N)^{3-}$ (Figure 3), particularly where the R group is a trialkylsilyl substituent. These bulky substituents afford excellent steric control over the open binding site on the metal center. The three NR_2^{1-} terminal groups and the neutral, apical R_3N group are "hard" and have proven particularly efficacious in binding "hard" early transition metals, including first-, second-, and third-row species such as vanadium, titanium, molybdenum, tantalum, and tungsten.[3]

Figure 3: Generic triamidoamine

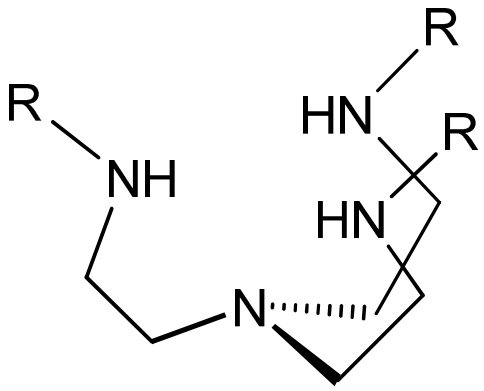

In contrast, the work of Schafer et al. has focused on amidate species bound to

metal centers. The amidate species is "softer": delocalization of the negative charge occurs between the N and O atoms of the amidate, potentially making these species more advantageous for "softer", late transition metals. Due in part to the delocalization of charge, the coordination chemistry of the amidate itself varies between four different general binding modes: it can take a monodentate form bound either through the O-donor atom or the N-donor atom; it can act as a bridging group; or it can chelate through both the N- and O-donor atoms (Figure 4). The binding mode adopted by the amidate is ultimately a combination of two factors. In its monodentate form, preferential O- or N-donor atom binding seems most directly related to the electronic character of the metal center: O-donor atom binding is preferential to the "hard" metals and N-donor atom binding to the "soft" metals.[4] At present most of the work that has been done with these ligand systems focuses on early transition metals and lanthanides as well, with some exceptions.

Figure 4: Binding modes of amidates[4]

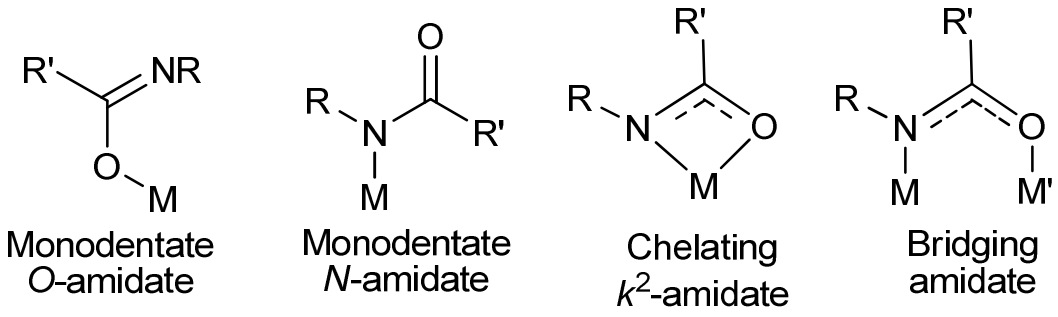

A steric preference also comes into play when dealing with the constraints of the ligand geometry, such as that of the tripodal ligand system. The bridging and chelating binding modes of the amidates are sterically unfavorable in such a geometry, and preferential binding can occur exclusively through the N-donor atoms.[4] The four N-donor

atoms typically chelate in a tetradentate manner, which creates a "pocket" for the metal center. This pocket is highly sterically encumbered, but can generate a fifth axial binding site on the metal center (Figure 5), the chemistry of which is dependent upon the steric and electronic effects generated by the character of the arms and the terminal groups attached to the amidates.[3]

Figure 5: "Pocket" binding of metal center

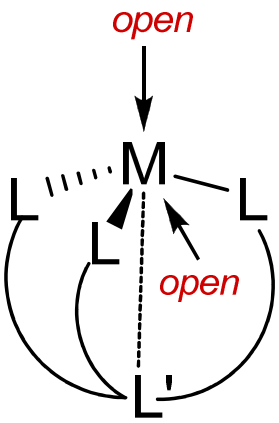

The tripodal triamidoamine structure offers several potential geometries for coordination complexes. Complexes utilizing the $[N_3N]^{3-}$ functionality have been reported in trigonal planar[5] and tetrahedral[6] geometries, as well as more uncommon trigonal mono- and bipyramidal[7] formations. The four- and five-coordinate trigonal monopyramidal (TMP) and trigonal bipyramidal (TBP) geometries are of particular interest because the coordination chemistry of the axial binding site of the metal center can be regulated through ligand design. This binding site can be selectively sterically protected: bulky terminal substituents on the amidates such as trialkylsilyl groups[7a] can keep the fifth binding site completely open, whereas groups of smaller bulk can allow the selective binding of halides, small linear molecules such as cyanide, larger coordinating solvents, or even possible dimerization.[7b]

As well as steric protection, the electronic character of the ligand offers the potential to tune the chemistry of the metal center. For instance, although simple hydrocarbon backbones can form mildly electron-donating ligands, enhancing electron density through the inclusion of aromatic structures could potentially lead to noninnocent or redox-active ligand behavior, such as in the case of *o*-phenylenediamine units[8] or *o*-phenylenediamine derivatives.[9]

We have chosen a ligand platform that incorporates *o*-phenylamine units instead of simple alkylamine units (Figure 6, Figure 7) in its arms for both steric and electronic reasons.[10] The steric bulk and constrained geometry of the phenylamine group should provide a less-flexible carbon backbone than an analogous alkylamine,[11] enhancing the steric protection achieved through the terminal amidates. The additional electron density from the aromatic moieties employed may incorporate ligand effects into the redox chemistry of the metal complexes. Lastly, while tetradentate tripodal analogs of the *o*-phenylamine donor of the form [N(*o*-PhL)$_3$] where L = OH[12] and PR$_2$[13] have been widely studied, the interactions of their amine counterparts with late-transition-metal species have not received attention in the literature.[14]

Within the basic ligand platform [N(*o*-PhNHC(O)R)$_3$], steric and electronic properties of the metal complexes can be tuned by alteration of the R substituent. We have sought to explore these different properties by varying both the steric bulk of the R-group (in a steric series where R = Me, ^{i}Pr, and C_6H_5) and by making it increasingly electron-withdrawing with regards to the electron-donating nature of the hydrocarbon substituents (with R = CF_3, *p*-$PhNO_2$, C_6F_5) (Figure 7).

Figure 6: [N(*o*-PhNH$_2$)$_3$] structure

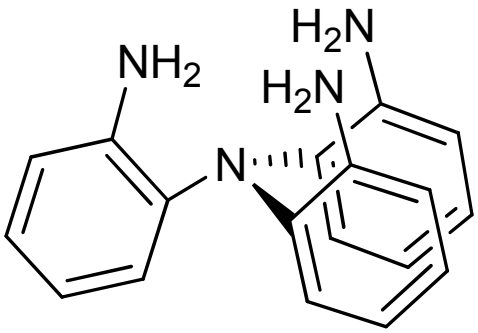

Figure 7: [N(*o*-PhNHC(O)R)$_3$] structures

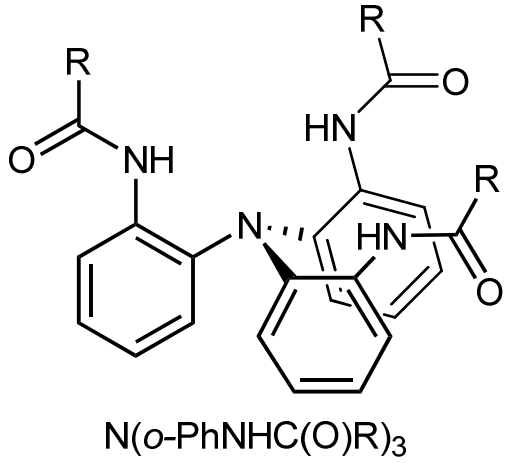

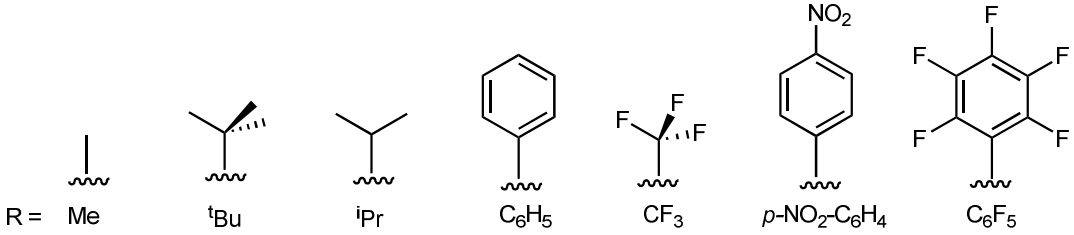

Investigation into the early-transition-metal and lanthanide complexes of tripodal tetradentate $(N_3N)^{3-}$ species has revealed unique functionalities in their chemistry. TMP complexes – with no ligand in the apical site of the metal center – formed from first row transition metals from titanium to iron have been characterized.[7a] Rarely seen species supported by the ligand system include terminal heavy-chalcogenide complexes,[15] a

tantalum phosphinidene species,[16] a titanium(IV) hydride,[17] and an iron(IV) cyanide species.[18] In addition, catalytic applications of molybdenum, manganese, and iron $(N_3N)^{3-}$ complexes have been reported.[19] The triamidoamine ligand system has proven especially useful in stabilizing low d-count metals as well as enabling terminal metal-ligand double- and triple-bonds at the apical binding site of the metal center – this has been verified in vanadium, tantalum, and tungsten complexes.[3]

Although the majority of current literature on the $[N_3N]^{3-}$ ligand systems involves early transition metal complexes, there are some notable corollaries with late transition metal species. Most readily notable is the case of iron, which has been reported in oxidation states III and IV in both TMP and TBP geometries.[17] In addition, iron(III) $[N_3N]^{3-}$ complexes in TBP geometry have been shown to stabilize terminal oxo and hydroxo ligands.[20] In addition, TMP complexes of high-spin iron(II), cobalt(II), nickel(II), and zinc(II) have been generated using the $[N_3N]^{3-}$ functionality.[21]

We have chosen to focus on the first-row late transition metal complexes of the $[N(o\text{-}PhNHC(O)R)_3]$ ligand set because their potential to form late transition metal complexes in high-spin, TMP geometry, and to stabilize double- or triple- terminal M-L bonds in an analogous manner to the known early transition metal species which perform this function.

Ongoing work by Matthew B. Jones has resulted in the synthesis of several late transition metal complexes with ligand structures from those listed in Figure 7, most notably complexes involving the R = ^{i}Pr and C_6H_5 structures. The metal species employed include iron, cobalt, nickel, aluminum, and zinc. Of these complexes, the nickel complex $[Ni(N(o\text{-}PhNHC(O)^{i}Pr)_3)]^{1-}$ (Figure 8) has proven the most interesting in

its electrochemistry. Cyclic voltammetry has indicated two reversible reductions in the nickel complex in its TMP geometry; in its TBP geometry, after binding cyanide, only one electrochemical event occurs. In addition, the X-band EPR spectrum indicates the presence of an unpaired electron which may be delocalized in the ligand structure as a result of noninnocent, redox-active ligand behavior. At present, we believe that the electron-donating effect of the R = ^{i}Pr derivative to the nickel center and its relatively lower steric bulk allow the possible noninnocent behavior of the ligand platform.

Figure 8: $[Ni(N(o\text{-}PhNC(O)^{i}Pr)_3)]^{1-}$

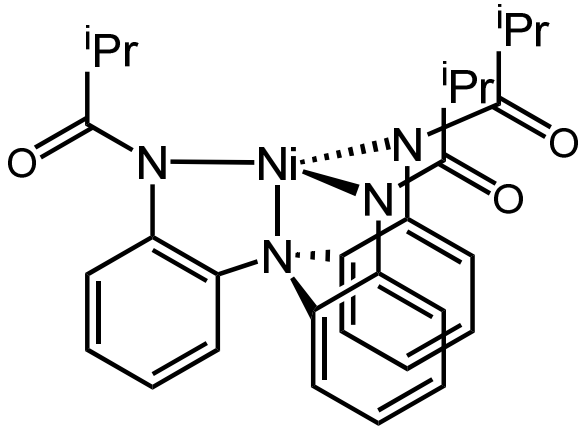

Work by Leslie Alexander resulted in the synthesis of an R = ^{t}Bu derivative of the ligand, but the steric bulk of the amidate substituents generated a “twisted”, non-C_3-symmetric geometry that incorporated an O-donor atom on one of the amidate “arms” in place of the usual N-donor atom (Figure 9). With regards to verifying the potentially noninnocent behavior of the ligand platform, steric bulk greater than the R = ^{i}Pr derivative is not desirable.

Figure 9: $[Ni(N(o\text{-}PhNC(O)^tBu)_3]^{-1}$

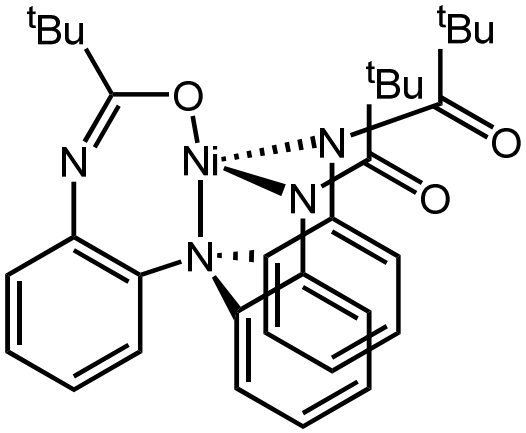

In this thesis I present the successful synthesis of the R = Me derivative (Figure 10), which completes the steric series of R = ^{i}Pr, ^{t}Bu, and C_6H_5, maintaining the electron-donating nature of these substituents without creating enough steric bulk to interfere with the amidate binding mode. I also report the successful synthesis of three metal complexes of this derivative, K[Co(N(*o*-PhNC(O)Me)$_3$)], K[Ni(N(*o*-PhNC(O)Me)$_3$)], and K[Zn(N(*o*-PhNC(O)Me)$_3$)]. While some spectroscopic data have been obtained to elucidate the features of these complexes, their characterization is incomplete due to an inability to obtain crystals of any metal complex. The functionality of these complexes and their comparison to data obtained on other, more fully characterized complexes in this ligand series is limited without a full understanding of their properties. However, the basic spectroscopic data reported confirms their synthesis and provides information related to the geometry of their structures.

Figure 10: [N(*o*-PhNHC(O)Me)$_3$]

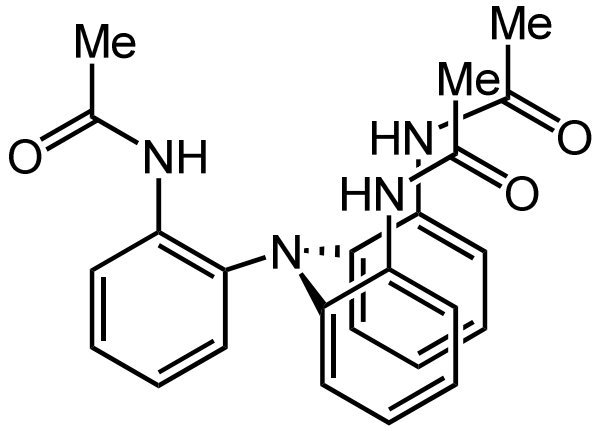

2. Experimental

The tetraamine ligand [N(*o*-PhNH$_2$)$_3$] was synthesized from the tris(2-nitrophenyl) precursor [N(*o*-PhNO$_2$)$_3$] (Figure 11) via a hydrogrenation reaction catalyzed by palladium. The [N(*o*-PhNO$_2$)$_3$] precursor was synthesized via an S_nAr reaction from the literature.[22] The tetraamine platform then underwent an acylation reaction with acetyl chloride to produce the R = Me derivative [N(*o*-PhNHC(O)Me)$_3$] (Figure 12). Metal complexes of the formula K[M(N(*o*-PhNC(O)Me)$_3$)] where M = Co, Ni, Zn and were then synthesized following a deprotonation of the ligand with KH and the addition of an $M^{II}X_2$ metal salt (Figures 13-15).[2]

General. Standard reagents purchased from Sigma-Aldrich were used for all syntheses. Purchased anhydrous solvents were sparged with argon gas and run through activated alumina columns. Synthesis of precursors was performed using standard Schlenk line techniques. Synthesis of metal complexes was undertaken in a Labmaster 130 dry box with a nitrogen atmosphere. All NMR spectra were recorded using a 400 Mhz INOVA NMR machine at ambient temperature. Proton and carbon spectra of the ligand were taken in $CDCl_3$ dried over activated molecular sieves. Spectra of complexes were recorded in DMSO-*d6*, which was purified by (1) drying over alumina and (2) distillation off of calcium hydride onto activated molecular sieves. All chemical shifts were referenced to residual solvent peaks. Mass spectra were recorded by the Emory University Mass Spectrometry Center using a JEOL JMS-SX102/SX102A/E mass spectrometer. Infrared spectra were recorded with a Varian Scimitar 800 Series FTIR spectrophotometer (KBr pellets). Electronic absorption spectra were recorded in 1.0 cm quartz cuvettes with a Cary 50 spectrophotometer. X-ray diffraction was recorded at the

Emory University X-ray Crystallography Laboratory using a Bruker Smart 1000 CCD diffractometer.

Figure 11: Synthesis of [N(*o*-PhNO$_2$)$_3$] and [N(*o*-PhNH$_2$)$_3$]

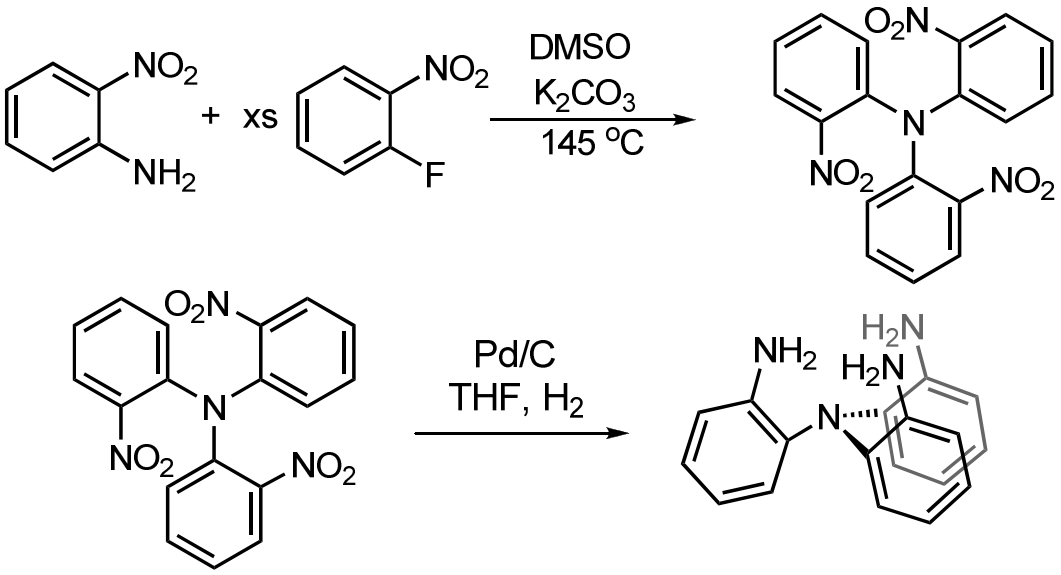

Synthesis of [N(*o*-PhNO$_2$)$_3$]. A 10.0 g sample of 2-nitroaniline (72.4 mmol) was dissolved in 50 mL of DMSO under an atmosphere of nitrogen with stirring. To this was added 30.5 mL of 2-fluoro-1-nitrobenzene (289.6 mmol) and 60.0 g of potassium carbonate (434.4 mmol). The reaction mixture was heated to 140 °C for and stirred for an additional 90 hours.

The reaction mixture was slowly cooled to room temperature, diluted to 1.0 L with H_2O, and filtered on a Buechner funnel to yield a dark yellow powder. This was stirred in a 1.0 L suspension of boiling MeOH for 30 minutes and filtered hot on a Buechner funnel. The resulting yellow powder was washed with MeOH and placed under vacuum for 24 hours to dry (68% yield). ^{1}H NMR (δ, $CDCl_3$, 300 Mhz): 7.84 (dd, 3H, ArH), 7.54 (td, 3H, ArH), 7.31 (td, 3H, ArH), 7.22 (dd, 3H, ArH). ^{13}C NMR (δ, $CDCl_3$, 300 Mhz): 143.95, 138.83, 134.02, 128.47, 126.42, 126.15. HRMS(ESI): $C_{18}H_{12}N_4O_6$ *m/z*

calcd. 381.08351 found 381.08352 $[M+1]^+$. FTIR (KBr, cm^{-1}): ν(NO) 1516, 1337. UV-Vis ($CHCl_3$) λ_{max}, nm (ε, M^{-1} cm^{-1}): 377 (4410).[23]

Synthesis of [N(*o*-PhNH$_2$)$_3$]. A 1.5 g (3.9 mmol) sample of crystalline [N(*o*-$PhNO_2)_3$] was dissolved in 50 mL of tetrahydrofuran in a pressure-safe reaction vessel. To this was added 0.85 g of Pd/C (0.7 mmol, 10 mol %). The reaction mixture was shaken under 50 psi of H_2 until consumption of H_2 ceased.

The reaction mixture was filtered on a pad of Celite to yield a light red solution. This was concentrated in vacuo to give a grey powder. The resulting power was taken up in a suspension of 20 mL of dichloromethane and stirred in a bath of dry ice and 2-propanol for 30 minutes. The suspension was then filtered cold and the resulting white powder was isolated on a frit and placed under vacuum for 24 hours to dry (83.3% yield). ^{1}H NMR (δ, $CDCl_3$, 300 Mhz): 6.99 (td, 3H, ArH), 6.92 (dd, 3H, ArH), 6.73 (dd, 3H, ArH), 6.71 (td, 3H, ArH), 3.70 (bs, 6H, NH). ^{13}C NMR (δ, $CDCl_3$, 300 Mhz): 143.36, 133.21, 126.40, 118.58, 116.65. HRMS(ESI): $C_{18}H_{18}N_4$ *m/z* calcd. 291.16097 found 291.16007 $[M+1]^+$. FTIR (KBr, cm^{-1}): ν(NH_2) 3455, 3360.[24]

Figure 12: Synthesis of [N(*o*-PhNHC(O)Me)$_3$]

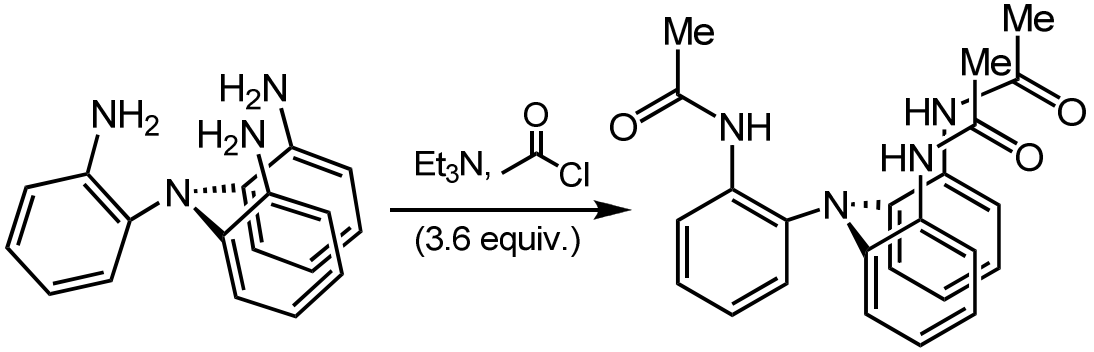

Synthesis of [N(*o*-PhNHC(O)Me)$_3$]. A 0.89 g (3.07 mmol) sample of [N(*o*-$PhNH_2)_3$] was dissolved in 40 mL of THF and placed in a dry ice and 2-propanol bath

under an atmosphere of nitrogen with stirring. To this was added 1.54 mL (11.04 mmol, 3.6 equiv.) of triethylamine, followed by 0.78 mL (11.04 mmol, 3.6 equiv.) of acetyl chloride. The reaction mixture was slowly warmed to room temperature and allowed to continue stirring for 20 hours.

The resulting reaction mixture was a white, opaque suspension. The reaction mixture was concentrated in vacuo and dissolved in 25 mL DCM, yielding a light green solution. This was washed 5 times with 50 mL of 0.1 M HCl and 3 times with 50 mL of deionized H_2O. The resulting solution was dried over magnesium sulfate and gravity filtered, then concentrated in vacuo to yield a light green oil.

The oil was triturated in hot hexanes to give a suspension of white powder. The suspension was chilled to settle the powder and filtered cold through a frit, isolating the white powder. This was washed with hexanes and placed under vacuum for 24 hours to dry (88.9% yield). ^{1}H NMR (δ, $CDCl_3$, 400 Mhz): 8.381 (s, 3H, NH), 7.651 (s, 3H, ArH), 7.080 (td, 6H, ArH), 6.806 (d, 3H, ArH), 1.727 (s, 9H, CH_3). ^{13}C NMR (δ, $CDCl_3$, 400 Mhz): 169.288, 138.495, 126.458, 126.065, 125.572, 125.187, 124.628, 23.416. HRMS(ESI): $C_{24}H_{24}O_3N_4$ *m/z* calcd. 417.19212 found 417.19201 $[M+1]^+$. FTIR (KBr, cm^{-1}): ν(NH) 3348, 3400, ν(CO) 1660.

Figure 13: Synthesis of K[Co(N(*o*-PhNC(O)Me)$_3$)]

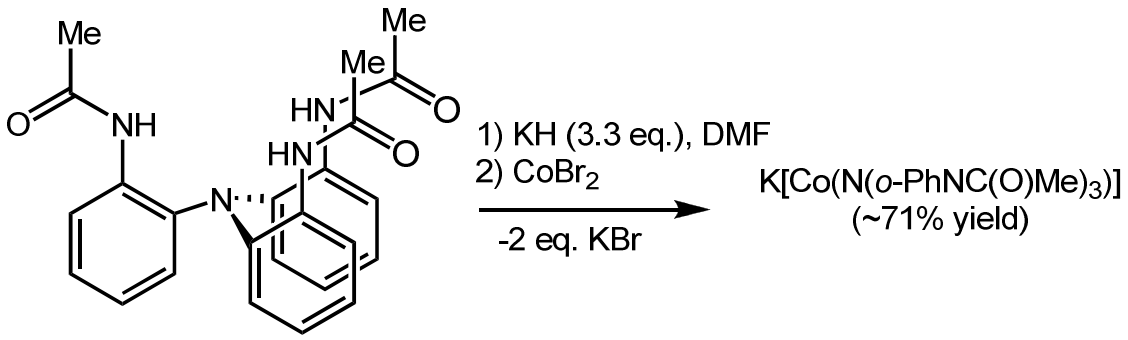

Synthesis of K[Co(N(*o*-PhNC(O)Me)$_3$)]. A 96.0 mg (0.23 mmol) sample of [N(*o*-PhNHC(O)Me)$_3$] was dissolved in 5 mL of DMF. To this was added 31.0 mg (0.76 mmol, 3.3 equiv.) of KH in a DMF slurry. Evolution of gas began immediately, and the reaction mixture was stirred for 12 hours until no more gas was evident and a white slurry formed. To this was added 51.3 mg (0.23 mmol) of $CoBr_2$ as a dark blue DMF solution. The reaction mixture immediately turned dark blue and was stirred for a further 6 hours.

The reaction mixture was filtered through a pad of Celite on a frit, resulting in a clear, dark blue solution. This solution was divided between two large (20 mL) vials and placed in a large jar full of diethyl ether. The ether was allowed to diffuse into the DMF solution for 48 hours, resulting in a dark blue powder.

The clear supernatant solution was decanted off the dark blue powder, which was collected with diethyl ether and isolated on a frit. The powder was washed heavily with diethyl ether and dried for several hours under vacuum (71% yield). ^{1}H NMR (δ, DMSO-*d6*, 400 Mhz): 48.996 (br), 46.145 (br), 42.170 (br), 31.770 (br), 21.098 (br), 13.863 (sh), 12.436 (br), 12.124 (br), 1.466 (br). FTIR (KBr, cm^{-1}): ν(CO) 1618, 1596. UV-Vis (DMF) λ_{max}, nm (ε, M^{-1} cm^{-1}): 566.1(83), 609.1(sh). HRMS(ESI): 472.09523 [M-1]$^-$.

Figure 14: Synthesis of K[Ni(N(*o*-PhNC(O)Me)$_3$)]

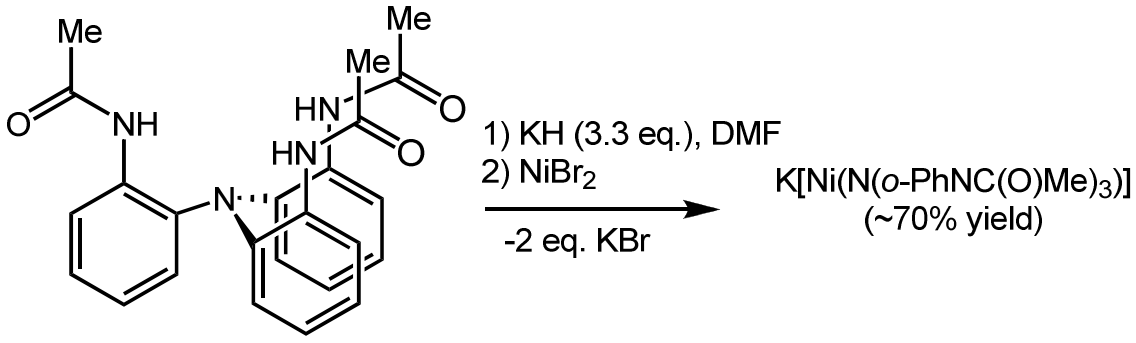

Synthesis of K[Ni(N(*o*-PhNC(O)Me)$_3$)]. A 96.0 mg (0.23 mmol) sample of [N(*o*-

PhNHC(O)Me)$_3$] was dissolved in 5 mL of DMF. To this was added 31.0 mg (0.76 mmol, 3.3 equiv.) of KH in a DMF slurry. Evolution of gas began immediately, and the reaction mixture was stirred for 12 hours until no more gas was evident and a white slurry formed. To this was added 50.3 mg (0.23 mmol) of $NiBr_2$ as an orange DMF slurry. The reaction mixture was stirred for a further 6 hours, by which point it had turned dark brown.

The reaction mixture was filtered through a pad of Celite on a frit, resulting in a clear, dark brown solution. This solution was divided between two large (20 mL) vials and placed in a large jar full of diethyl ether. The ether was allowed to diffuse into the DMF solution for 48 hours, resulting in a light orange powder.

The clear supernatant solution was decanted off the light orange powder, which was collected with diethyl ether and isolated on a frit. The powder was washed heavily with diethyl ether and dried for several hours under vacuum (70% yield). ^{1}H NMR (δ, DMSO-*d6*, 400 Mhz): 25.278 (br), 22.234 (br), 18.752 (br), 16.142 (sh), 14.110 (br), 13.241 (sh), 11.353 (br), 1.655 (br), -2.421 (br), -4.017 (br), -6.197 (br), -15.040 (br), -16.346 (br). FTIR (KBr, cm^{-1}): ν(CO) 1630, 1596. UV-Vis (DMF) λ_{max}, nm (ε, M^{-1} cm^{-1}): 400.5 nm (sh), 690.0(16). HRMS(ESI): 471.09740 [M-1]$^-$.

Figure 15: Synthesis of K[Zn(N(*o*-PhNC(O)Me)$_3$)]

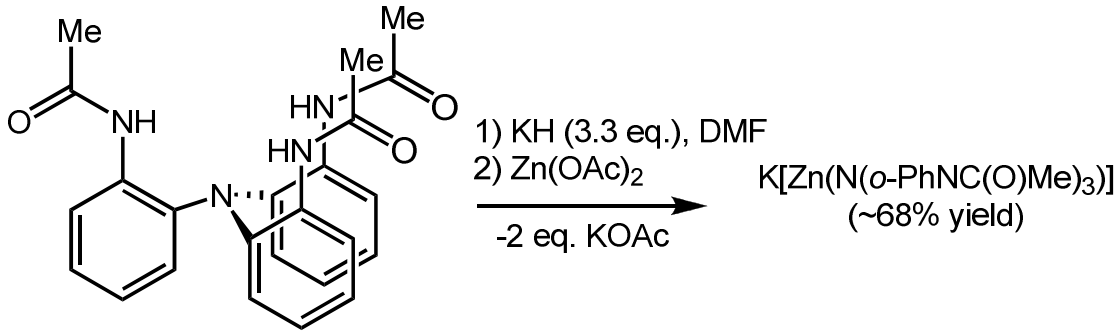

Synthesis of K[Zn(N(*o*-PhNC(O)Me)$_3$)]. A 96.0 mg (0.23 mmol) sample of

[N(*o*-PhNHC(O)Me)$_3$] was dissolved in 5 mL of DMF. To this was added 31.0 mg (0.76 mmol, 3.3 equiv.) of KH in a DMF slurry. Evolution of gas began immediately, and the reaction mixture was stirred for 12 hours until no more gas was evident and a white slurry formed. To this was added 42.2 mg (0.23 mmol) of $Zn(OAc)_2$ (OAc = acetate) as a white DMF slurry. The reaction mixture immediately turned clear and was stirred for a further 3 hours.

The reaction mixture was filtered through a pad of Celite on a frit, resulting in a clear solution. This solution was divided between two large (20 mL) vials and placed in a large jar full of diethyl ether. The ether was allowed to diffuse into the DMF solution for 48 hours, resulting in a white powder.

The clear supernatant solution was decanted off the white powder, which was collected with diethyl ether and isolated on a frit. The powder was washed heavily with diethyl ether and dried for several hours under vacuum (68% yield). ^{1}H NMR (δ, DMSO-*d6*, 400 Mhz): 7.199 (s, 3H, ArH), 6.804 (t, 3H, ArH), 6.680 (dd, 4H, ArH), 1.747 (s, 3H, CH_3), 1.511 (s, 6H, CH_3). ^{13}C NMR (δ, DMSO-*d6*, 400 Mhz): 172.158, 169.396, 146.912, 143.098, 127.249, 125.824, 123.297, 120.656, 26.168, 15.826. FTIR (KBr, cm^{-1}): ν(CO) 1595, 1576. HRMS(ESI): 477.09111 $[M-1]^-$.

3. Results and Discussion

General. Confirmation of the structural details of [N(*o*-PhNHC(O)Me)$_3$] **(1)** was obtained through ^{1}H and ^{13}C NMR, FTIR, and mass spectrometry. A crystal structure of acidified ligand H_3O[N(*o*-PhNHC(O)Me)$_3$]]Cl **(2)** was isolated from an acid wash of the initial reaction mixture. All spectroscopy data on **1** are presented in Appendix A.

Spectroscopic identification of the metal complexes of **1** was hindered by an inability to crystallize any of the three complexes K[Co(N(*o*-PhNC(O)Me)$_3$)] **(3)**, K[Ni(N(*o*-PhNC(O)Me)$_3$) **(4)**, and K[Zn(N(*o*-PhNC(O)Me)$_3$) **(5)**. Attempts at crystallization were generally hindered by the solubility properties of all three complexes. The complexes are completely soluble in N,N-dimethylformamide (DMF), but minimally soluble in any other solvent which could be used as a crystallizing agent – acetonitrile (MeCN), dichloromethane (DCM), tetrahydrofuran (THF), and benzene. Diffusion crystallizations of diethyl ether into DMF on both the small scale (small vial in large vial method) and large scale (large vial in jar method) resulted in the deposition of a powder. Other crystallization techniques employed were the diffusion of diethyl ether into MeCN; layering of hexanes on DCM; layering of diethyl ether on THF, MeCN, and DMF; and thermal gradient crystallization from warm benzene, DCM, THF, MeCN, and DMF. In all instances except that of DMF the complexes have low enough solubility that powder deposited within an hour. In DMF the complex remains so soluble that the only effective method of isolation was the diffusion of diethyl ether, which again resulted in the deposition of a powder.

In addition to different crystallization techniques, counterion variation was employed in an attempt to enhance the formation of crystalline material. Both size and

symmetry of cations were varied, but with no resultant crystals. Salt metatheses employed for **3** and **4** included the use of potassium (K^+), tetraethylammonium (Et_4N^+), tetraphenylphosphonium (Ph_4P^+), trimethylphenylammonium (Me_3PhN^+), and bis(triphenylphosphoranylidene)ammonium (PNP^+) salts, none of which resulted in the formation of crystalline material. For **3**, the stoichiometry of the salt metathesis was also varied from 1 to 2 equivalents of the counterion salt, which resulted in no change to the character of the deposited powder. In the case of **5**, salt metathesis employed included potassium (K^+), tetraethylammonium (Et_4N^+), and tetraphenylphosphonium (Ph_4P^+) salts. When powder deposited out of the diffusion of diethyl ether into DMF, however, none of the counterions employed were incorporated into the complex. Instead, a potassium salt complex codeposited with crystalline counterion, which were separated by washing.

For complexes **3** and **4**, spectroscopic data obtained includes paramagnetic ^{1}H NMR, FTIR, electronic absorption spectroscopy, and negative ion ESI mass spectrometry. These data are presented in Appendices B and C respectively. For complex **5**, spectroscopic data obtained includes diamagnetic ^{1}H and ^{13}C NMR, FTIR, and negative ion ESI mass spectrometry. These data are presented in Appendix D.

Structural details of [N(*o*-PhNHC(O)Me)$_3$]. The expected C_3-symmetric molecule is confirmed by both ^{1}H and ^{13}C NMR. In the proton NMR, the methyl singlet at 1.727 ppm and amide singlet at 8.381 ppm indicate equivalency of the protons in each of the three arms. Similarly, the integrations of the aromatic region suggest equivalency of the four protons involved in each of the three aromatic rings of the carbon backbone. The ^{13}C NMR confirms this with a single peak at 23.416 ppm for the methyl carbon; a single peak at 169.265 ppm for the carbonyl carbon; and six distinct peaks between 125

and 138 ppm for the aromatic carbons.

The FTIR of **1** indicates the presence of the expected N-H amide stretches in the 3100-3500 cm^{-1} region as well as the N-H amide bend at $\nu_{(NH)}$ = 1594 cm^{-1}. Aromatic C-H stretches are present between 3000-3100 cm^{-1}, and aromatic C=C stretches present between 1400-1600 cm^{-1}. The carbonyl stretch is indicated at $\nu_{(CO)}$ = 1660 cm^{-1}, consistent with an amide carbonyl stretch.

Mass spectrometry indicates that the calculated *m/z* ratio of the complex is 417.19212 and the found *m/z* ratio is 417.09201, with δ = -.26.

During the washing procedure outlined above, the acidified complex **2** was isolated from a suspension in .1 M HCl. The powder isolated was dark grey in color and was crystallized by diffusion of diethyl ether into methanol through the large vial in jar method; the resulting crystal was translucent gray and cubic in shape. The crystal structure of this complex is given in Figure 16.

Figure 16: Thermal ellipsoid diagram of **2**

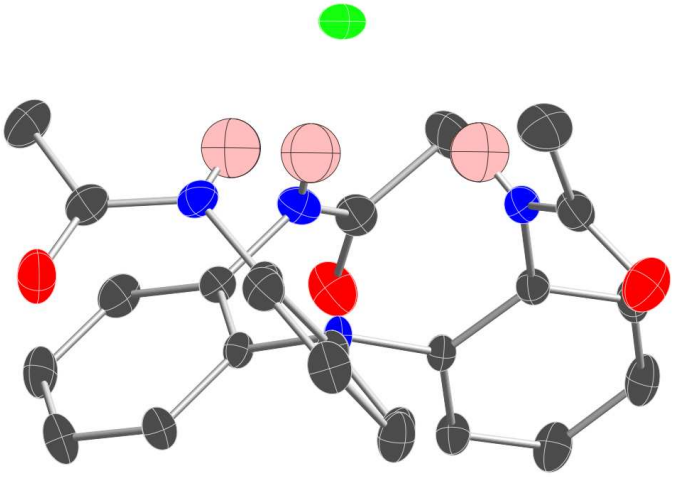

Figure 12: The hydronium counterion and all protons except the amide protons have been omitted for clarity. Grey = carbon, blue = nitrogen, red = oxygen, green = chlorine, pink = hydrogen.

The amide proton-chlorine ion distance in the structure of **2** is 2.365 A, close enough to suggest a hydrogen bonding interaction between the two. Although no crystal structures were obtained for metal complexes **3**, **4**, and **5**, the structure of **2** gives an analog to the anticipated "pocket" binding of metal centers through its hydrogen-bonding of the chlorine ion. The molecule has C_3-symmetry and chelates the ion in a tridentate fashion through the three amide protons. The crystal data and refinement parameters of the structure are given in Table 1.

Table 1: Crystal data and refinement parameters of **2**

Empirical formula	$C_{24}H_{27}ClN_4O_4$
Formula weight	470.95 (g/mol)
Temperature	173(2) K
Wavelength	0.71073 A
Crystal system	Trigonal
Space group	P-3c1
Unit cell dimensions	a = 11.017(7) A, α = 90°
	b = 11.017(7) A, β = 90°
	c = 26.100(17) A, γ = 120°
Volume	2743(3) A^3
Z	4
Density (calculated)	1.140 Mg/m^3
Absorption coefficient	0.172 mm^{-1}
F(000)	992
Crystal size	0.17 x 0.17 x 0.14 mm^3
Theta range for data collection	1.56 to 30.45°
Index ranges	-15<=h<=14, -15<=k<=15, -36<=l<=36
Reflections collected	45843
Independent reflections	2757 [R(int) = 0.0602]
Completeness to theta = 30.45°	98.9%
Absorption correction	Semi-empirical from equivalents
Max. and min. transmission	0.9763 and 0.9714
Refinement method	Full-matrix least-squares on F^2
Data/restraints/parameters	2757/0/112
Goodness-of-fit on F^2	1.069
Final R indices [I>sigma(I)]	R1 = 0.0498, wR2 = 0.1452
R indices (all data)	R1 = 0.0653, wR2 = 0.1548
Largest diff. peak and hole	0.406 and -0.306 $e.A^{-3}$

The crystal structure indicates the carbonyls of the ligand arms engage in hydrogen-bonding through the protons of the hydronium molecules with a bond distance

of 1.579 A, generating a lattice arrangement depicted in Figure 17.

Figure 17: Lattice view of **2**

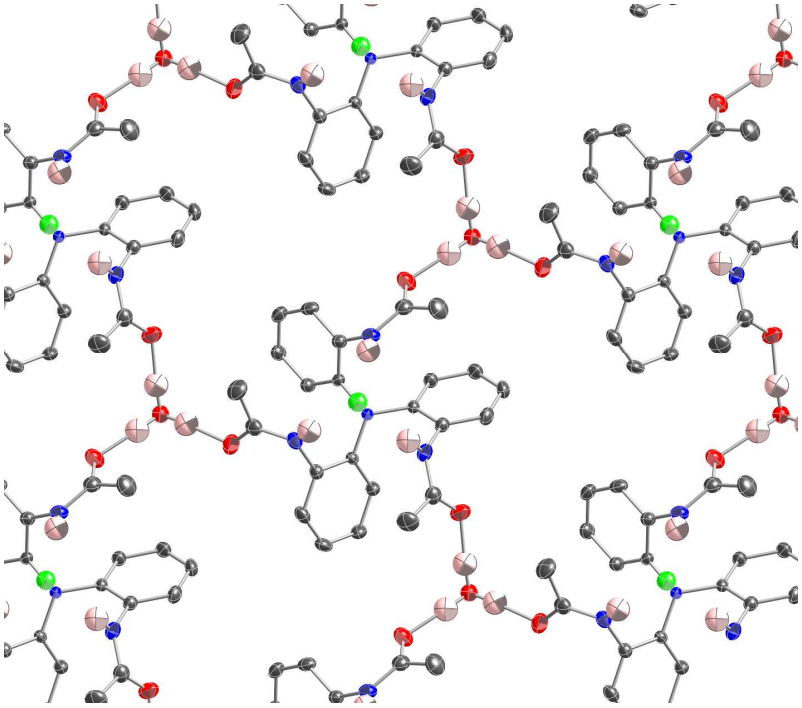

Figure 17: Lattice view of **2**. Carbonyl O-donors hydrogen bond through the hydronium proton with a bond distance of 1.579 A.

Structural details of K[Co(N(*o*-PhNC(O)Me)$_3$)] (3). Spectroscopic data gathered indicates the formation of the desired complex. However, due to a lack of crystalline material, structural elucidation of **3** remains incomplete.

The negative ion ESI MS of **3** suggests successful formation of the complex with a parent peak at 472.09523 *m/z* which correlates to the $[M-1]^-$ *m/z* of the cobalt complex with no counterion.

Paramagnetic ^{1}H NMR indicates that the resulting complex is paramagnetic, as would be expected from a high-spin d^7 cobalt(II) complex. Beyond this feature, the NMR is inconclusive. The presence of 5 paramagnetic peaks is expected for a C_3-symmetric complex, which follows from a paramagnetic shift of the four aromatic protons in one

aromatic ring of the backbone and the protons of the methyl group on one of the arms. The spectrum reveals large paramagnetic peaks at 13.863 ppm and 31.770 ppm. These peaks are similar to those found in the paramagnetic proton NMR of the R = ^{i}Pr species.

Aside from these peaks, however, other paramagnetic peaks are small and possibly indeterminate; in addition, if all possible paramagnetic peaks shown in the spectrum are counted, there are 7-10 peaks. This may indicate a lowering of the C_3-symmetry to C_s-symmetry, as would be the case if one arm were rotated so that the amidate binding occurs through the O-donor rather than the N-donor atom (shown in Figure 17). O-donor binding has been observed in the R = ^{t}Bu, under opposing circumstances: the steric bulk of the terminal groups prohibited effective binding of all three N-donors and caused one arm to "splay" outwards, whereas in the case of the R = Me ligand, it would be lack of steric hindrance which causes this to occur. If this is the case, 10 paramagnetic peaks are predicted – five for the four aromatic protons and one for the methyl protons on the two symmetric arms, and an additional five for the four aromatic protons and one for the methyl protons on the rotated arm. This possibility cannot be entirely discounted due to the number of apparent paramagnetic peaks and the chance that other peaks are obscured or are too low an intensity to be located from a powder sample of **3**.

Figure 18: Alternate structure of **3** (C_s-symmetry)

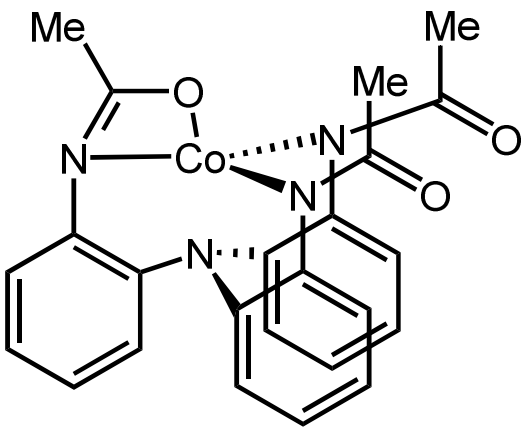

Complex dimerization may also explain the nature of the obtained spectroscopy. This possibility is not precluded from the mass spectrum of the complex, as the charge-to-mass ratio would remain the same in the dimer, and a C_2-symmetric dimer complex would likewise have 10 peaks in its proton NMR spectrum. The reduction of steric bulk associated with the R = Me ligand might promote dimerization, whereas the enhanced steric bulk of larger derivatives (R = ^{i}Pr, ^{t}Bu, Ph) would prevent this phenomenon. Although dimerization has not been observed with a Co(II) complex of any of the ligand derivatives, the Zn(II) complex of the R = ^{i}Pr derivative has been characterized as a dimer by X-ray crystallography. A proposed structure for what an R = Me dimer of the Co(II) complex is given in Figure 18.

Figure 19: Alternate structure of **3** (C_2-symmetry)

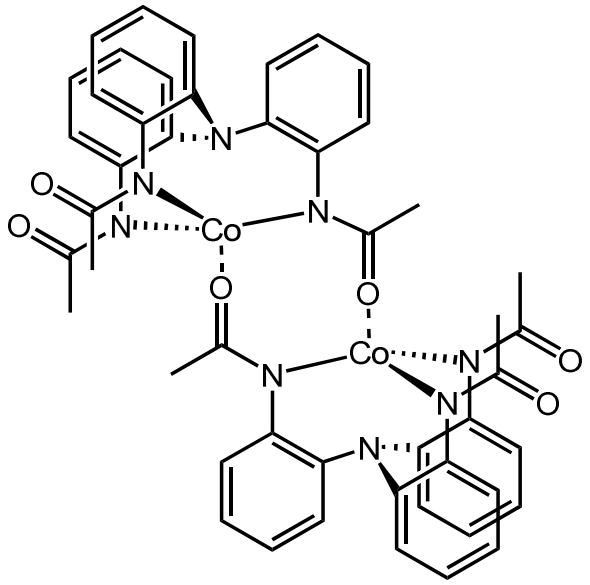

FTIR data of **3** suggest formation of the desired cobalt complex. The N-H stretches apparent in the FTIR of **1** are absent, suggesting successful deprotonation of the amides by the KH. In addition, the carbonyl stretch has shifted from $\nu_{(CO)}$ = 1660 cm^{-1} to $\nu_{(CO)}$ = 1618 cm^{-1}, consistent with a literature values for an N-bound amidate C=O stretch on a Co(II) center[25] near 1620 cm^{-1}, and with carbonyl stretches observed in other ligand derivatives.. The presence of an additional carbonyl stretch at $\nu_{(CO)}$ = 1596 cm^{-1} may suggest a second carbonyl environment, supporting the NMR findings of a potentially C_s-symmetric or C_2-symmetric species rather than a C_3-symmetric species. This value agrees with literature values between 1560 and 1600 for and amidate O-donor species[26].

Both the NMR and IR confirm the presence of DMF in the sample. Literature values[27] for $\nu_{(CO)}$ of DMF bound to a Co(II) center place the frequency near 1650 cm^{-1}. However, the DMF carbonyl in the FTIR of **3** has a $\nu_{(CO)}$ = 1664, suggesting it is not coordinating to the metal center. This supports a trigonal monopyramidal geometry for **3**

which leaves open the axial binding site on the cobalt center.

Electronic absorption spectroscopy shows an absorption at 566.1 nm, which corresponds to an amide metal-to-ligand charge transfer (MLCT), and a shoulder at 609.1 nm, which corresponds to an amine ligand-to-metal charge transfer (LMCT). These correlate with observed phenomena in other ligand cobalt complexes and suggest the successful formation of a cobalt(II) complex.

Structural details of K[Ni(N(*o*-PhNC(O)Me)$_3$)] (4). Proton NMR data on complex **4** are less conclusive than the data obtained for **3**. While the spectrum is paramagnetic, as is expected for a high-spin d^8 nickel complex, the predicted number of peaks is either 5 for a C_3-symmetric species or 10 for a C_s-symmetric or C_2-symmetric species, as discussed above. However, the spectrum reveals significantly more than 10 peaks in total, with numerous overlapping and indeterminate peaks between 10 and 20 ppm. The complex may be undergoing a fluxional process in solution which gives rise to the profusion of paramagnetic peaks, but this has not been confirmed.

More positive data has been obtained from other characterization efforts. Mass spectrometry shows a parent peak at 471.09740 *m/z* corresponding to the $[M-1]^-$ *m/z* of the nickel complex with no counterion. This does not delineate between the formation of a monomeric or dimeric complex, however.

FTIR of **4** shows the predicted absence of N-H stretches as a result of deprotonation, and a carbonyl peak at $\nu_{(CO)}$ = 1630 consistent for literature values between 1610 and 1640 cm^{-1} for an N-bound amidate[28]. The DMF carbonyl peak at $\nu_{(CO)}$ = 1669 suggests that the DMF in the sample is not coordinated with the complex, as literature values are between 1650 and 1660 for other Ni(II) species[29], which predicts a

TMP geometry for the complex. An additional peak at 1596 cm^{-1} corresponds to a second C=O stretch in agreement with literature values for an O-bound amidate on a Ni(II) species[30] between 1570 and 1600 cm^{-1}, potentially indicating a rearrangement of the ligand arms to C_s- or C_2-symmetry.

The electronic absorption spectrum of **4** shows a shoulder at 396.4 nm which corresponds to the predicted amide metal-to-ligand charge transfer (MLCT), and an absorption at 690.4 nm which corresponds to the amine ligand-to-metal charge transfer (LMCT). These phenomena further suggest the successful formation of the Ni(II) complex.

Structural details of K[Zn(N(*o*-PhNC(O)Me)$_3$)] (5). Complex **5** is a diamagnetic d^{10} zinc complex, making it significantly easier to identify through ^{1}H and ^{13}C NMR techniques. The proton NMR of **5** shows an absence of the amide proton peak present in the proton NMR of **1** at 8.381, indicating successful deprotonation of the ligand. A more interesting feature of the spectrum, however, is the two methyl peaks at 1.511 and 1.747 ppm, which integrate in a 2:1 ratio. Although the paramagnetic spectra of **3** and **4** offer no clear information on the structure of those complexes, the two methyl peaks in the proton NMR of **5** suggests a confirmation of an alternate geometry for the complex: either a C_s-symmetric species with a mixed N- and O-donor binding mode, or else a dimeric complex. This phenomenon has an analog in the R = ^{i}Pr ligand, the Zn(II) complex of which is known to dimerize and has been characterized by X-ray crystallography. The data of the proton NMR spectrum are corroborated by the ^{13}C NMR of **5**, which indicates two peaks at 172.158 and 169.396 ppm for the two carbonyl carbon environments, and two peaks at 26.168 and 15.826 ppm for the two methyl carbon

environments.

The FTIR of **5** offers similar findings. As expected from a deprotonated complex, there are no N-H stretches present. In addition, there is a carbonyl stretch at $\nu_{(CO)}$ = 1595 cm^{-1}, which falls in a literature range near 1600 cm^{-1} for an N-bound amidate in a Zn(II) complex[31] and a second peak at $\nu_{(CO)}$ = 1576 cm^{-1}, in the literature range between 1560 and 1580 cm^{-1} for an O-bound amidate[32], supporting the presence of two carbonyls in different environments. The DMF carbonyl stretch at $\nu_{(CO)}$ = 1670 indicates that the DMF is not coordinated to the zinc complex as it does not agree with published values between 1630 cm^{-1} and 1650 cm^{-1}.[33] This supports a trigonal monopyramidal geometry for the zinc complex. This is corroborated by the presence of DMF in the proton NMR, which should integrate in a 1:1 ratio with the 6H proton peak at 1.511 ppm. This is not the case, however, suggesting that there is less than a 1:1 ratio of DMF to complex.

Mass spectrometry confirms the successful synthesis of the zinc complex with a parent peak at 477.09111 *m/z* which corresponds to the $[M-1]^-$ *m/z* of the complex with no counterion. However, these data do not differentiate between the possibilities of the C_s-symmetry complex or the C_2-symmetry dimer.

Characterization considerations. Mass spectrometry of **3, 4**, and **5** is the most consistent and conclusive positive indicator that the desired complexes are forming. However, mass spectrometry data cannot confirm whether the monomeric, "rotated" C_s-symmetry species has been synthesized, or whether a dimeric complex of equivalent charge-to-mass ratio is the preferred product. In seeking to resolve the question of dimerization, variations in reaction stoichiometry (for both 1:2 and 2:1 equivalents of ligand to metal) produced no positive results. The mass spectrum of complex **5** indicates

significant peaks at *m/z* ratios at around double the parent $[M-1]^-$ peak at 917.38838 and 987.35154 *m/z*, but no further evidence of dimerization was found in any complex.

In addition, the potential for fluxional behavior, particularly in complex **4**, was considered, but the solubility properties of the complex make resolution through low-temperature NMR difficult. The only deuterated solvent in which **4** appears to be soluble at sufficient concentrations is DMSO-*d6*, which has a freezing point too low to be an effective NMR solvent for low-temperature fluxional studies.

Based on the consistent IR data of all three complexes, it is reasonable to assume that **3**, **4,** and **5** exist as four-coordinate complexes of the late transition metals. If the complexes are not dimerizing, they exist in a TMP geometry with the fifth axial binding site open, and as indicated by the two carbonyl stretches of each species in a C_s-symmetry formation with a "rotated" arm acting as an O-donor rather than an N-donor. In the case of the dimer, using the R = ^{i}Pr zinc complex as an analog, it is likely that the species remains four-coordinate, with the metal center coordinated to the carbonyl oxygen of an arm of the other monomer but no binding through the apical nitrogen (as represented in Figure 15). The symmetry and binding mode of the amidates in the cases of complex **3** and **4** remains indeterminate without more definitive spectroscopy.

The departure from C_3-symmetry geometry of complex **5** is more conclusively defined due to the diamagnetism of the zinc center, which allows ^{1}H and ^{13}C NMR and IR to be corroborated with one another. It is not clear from the data whether the complex has adopted the C_s- or C_2-symmetric geometries. The dimeric possibility appears to corroborate with the behavior of the R = ^{i}Pr zinc complex, but beyond this information it is difficult to predict why the preferential formation of an alternate geometry for this

complex occurs.

Future directions. The addition of a strong donor ligand to the complexes may help to ascertain whether complex dimerization is responsible for the difficulty in crystallizing metal complexes **3**, **4**, and **5** and the unresolved question of their symmetry. A strong donor would presumably occupy the empty binding site on the metal centers and would interfere with the formation of a dimer, hopefully with a five-coordinate monomer species as the preferred result. Steric hindrance would be a consideration in selecting a donor, as a suitably large ligand would facilitate the monomerization, but too large a ligand may not be able to access the sterically protected binding site and dimer formation may occur preferentially.

Fluxional studies, particularly of complex **4**, would be of help in resolving the excess of peaks present in the proton NMR spectrum. The most accessible of these would be low-temperature NMR, but as mentioned above solvent choice limits the availability of solvents with which to perform this technique. DMF-*d7* would likely be the most useful solvent, but due to its excessive cost no fluxional studies have been performed on these complexes.

Appendix A. Spectroscopic Data on [N(*o*-PhNHC(O)Me)$_3$].

1. ^{1}H NMR of [N(*o*-PhNHC(O)Me)$_3$].

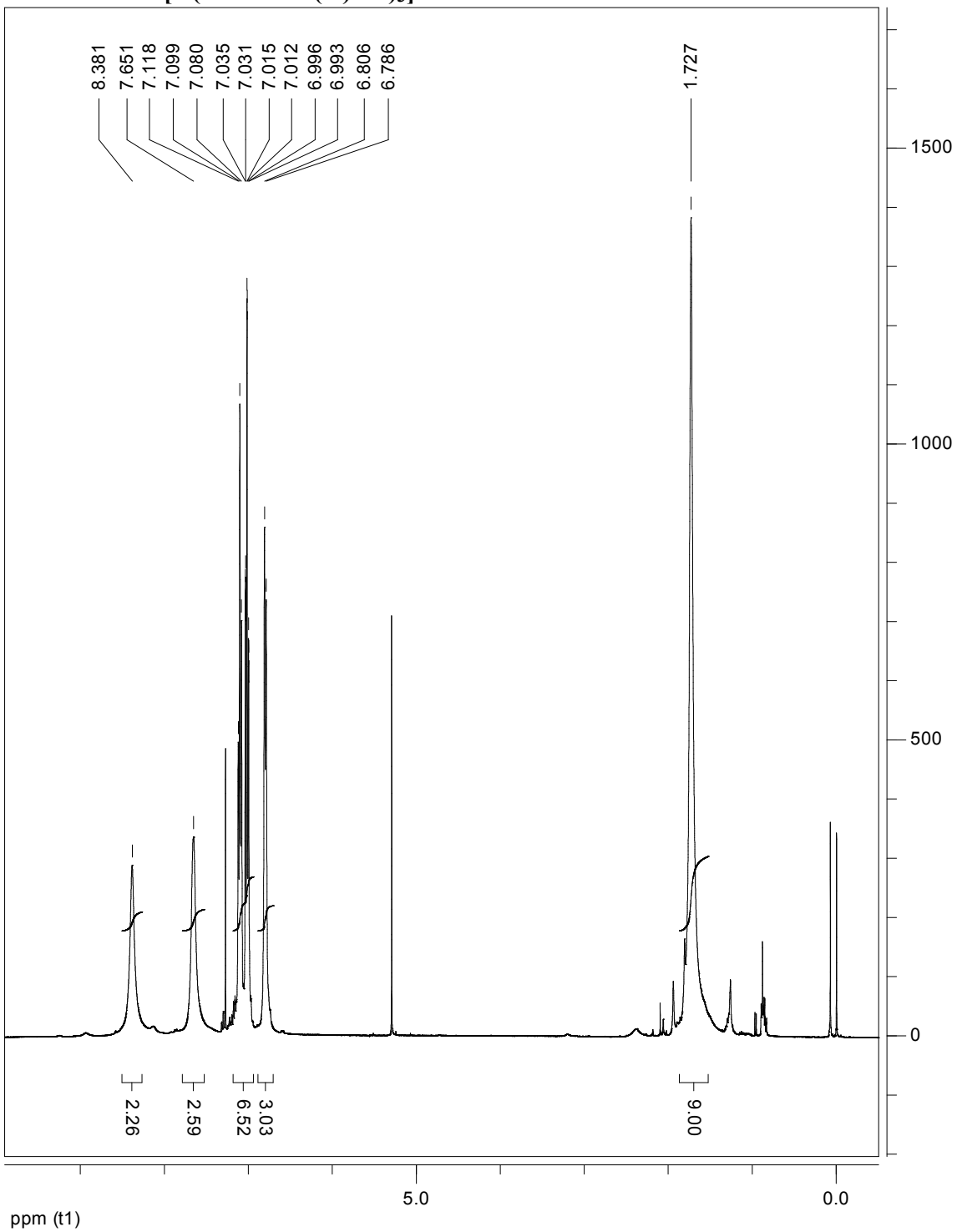

2. ^{13}C NMR of [N(*o*-PhNHC(O)Me)$_3$].

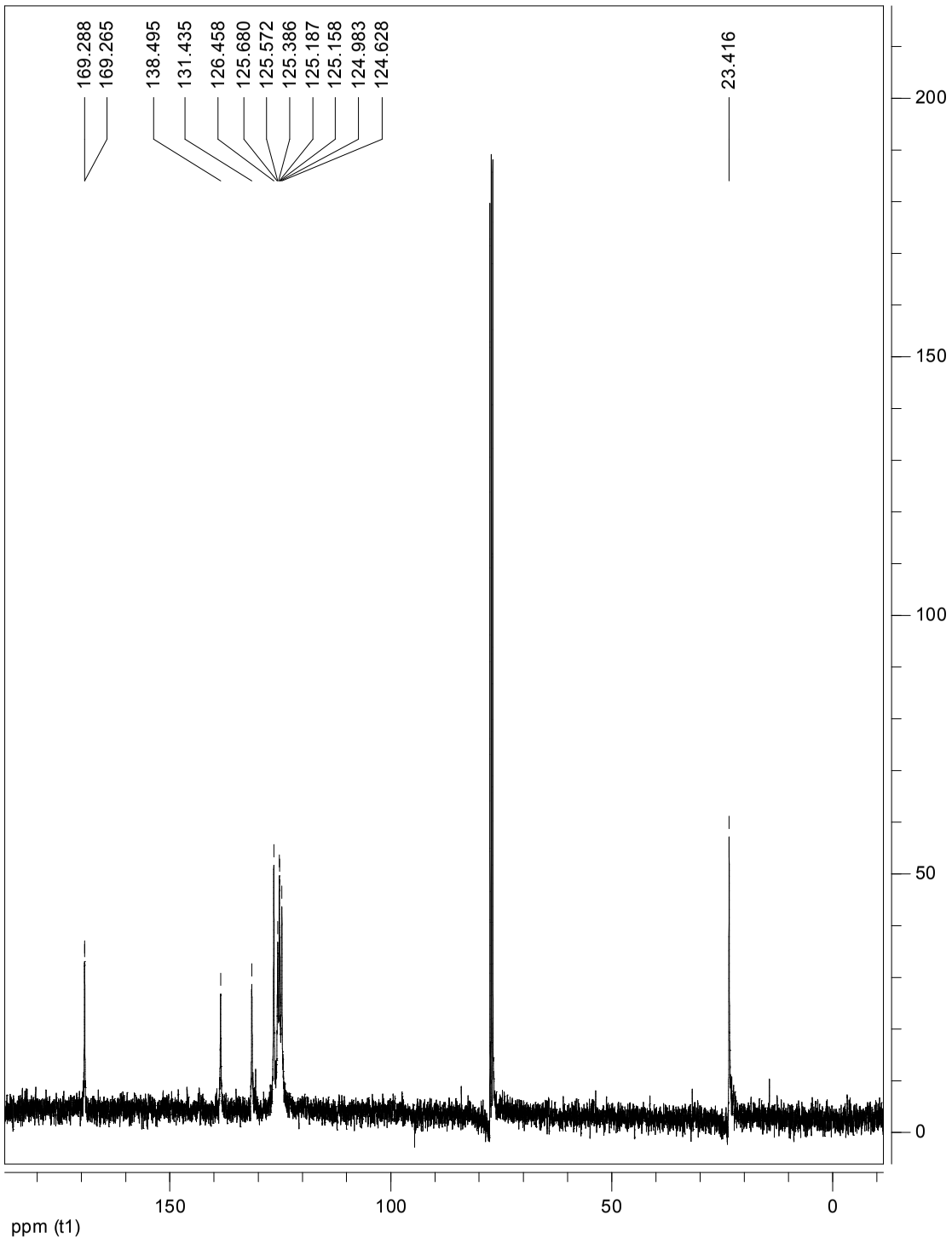

3. FTIR of [N(*o*-PhNHC(O)Me)$_3$].

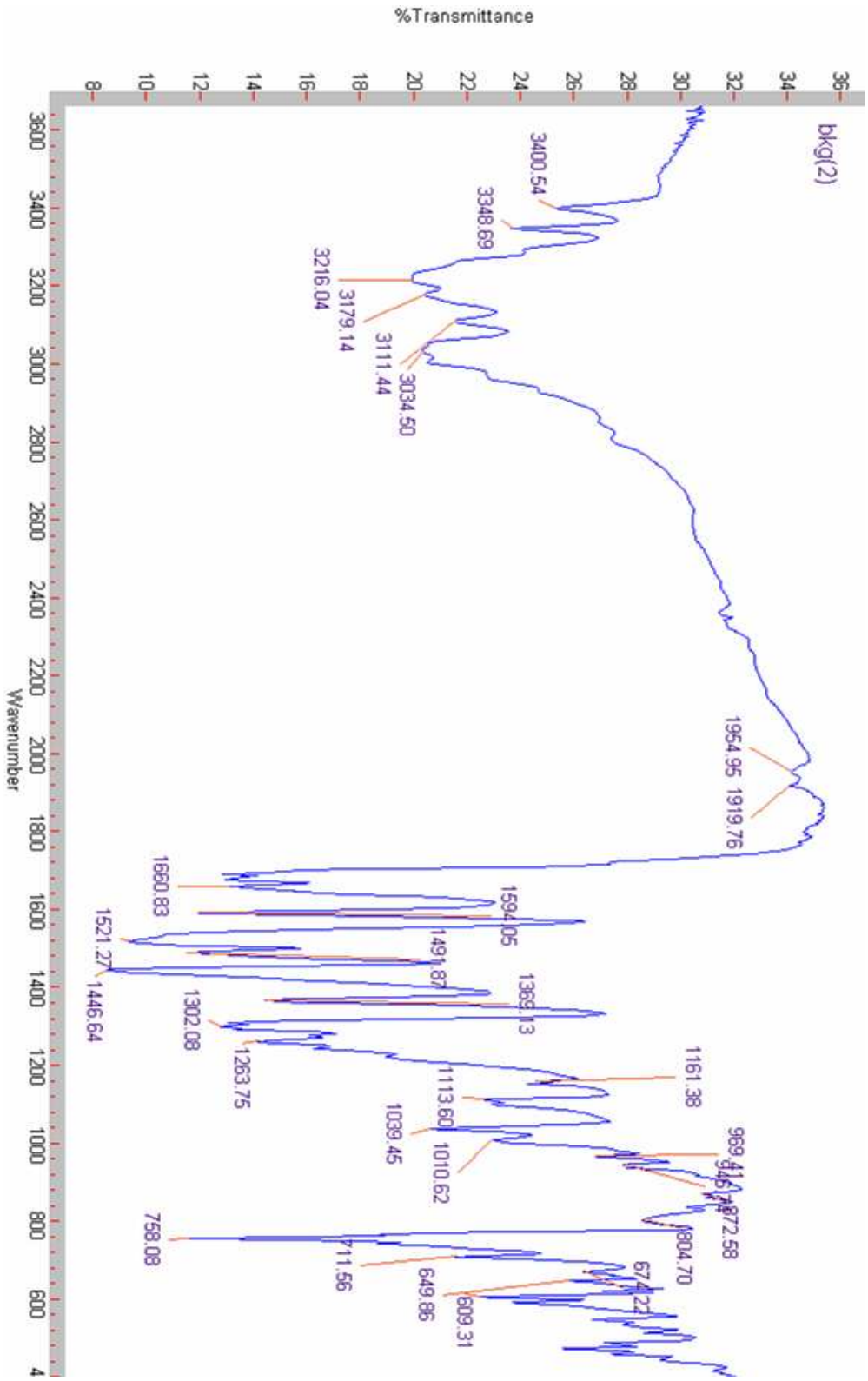

4. Exact mass MS of [N(*o*-PhNHC(O)Me)$_3$].

Elemental composition search on mass 417.19201

m/z= 412.19201-422.19201

m/z	Theo. Mass	Delta (ppm)	RDB equiv.	Composition
417.19201	417.19212	-0.26	14.5	$C_{24}H_{25}O_3N_4$
	417.19263	-1.48	2.0	$C_{10}H_{27}O_9N_9$
	417.19078	2.95	9.5	$C_{23}H_{29}O_7$
	417.19077	2.96	15.0	$C_{22}H_{23}O_2N_7$
	417.19346	-3.48	14.0	$C_{26}H_{27}O_4N_1$
	417.19397	-4.69	1.5	$C_{12}H_{29}O_{10}N_6$
	417.18944	6.17	10.0	$C_{21}H_{27}O_6N_3$
	417.18943	6.18	15.5	$C_{20}H_{21}O_1N_{10}$
	417.19480	-6.68	19.0	$C_{27}H_{23}N_5$
	417.19531	-7.90	6.5	$C_{13}H_{25}O_6N_{10}$

Appendix B. Spectroscopic Data on K[Co(N(*o*-PhNC(O)Me)$_3$)].

1. Paramagnetic ^{1}H NMR of K[Co(N(*o*-PhNC(O)Me)$_3$)].

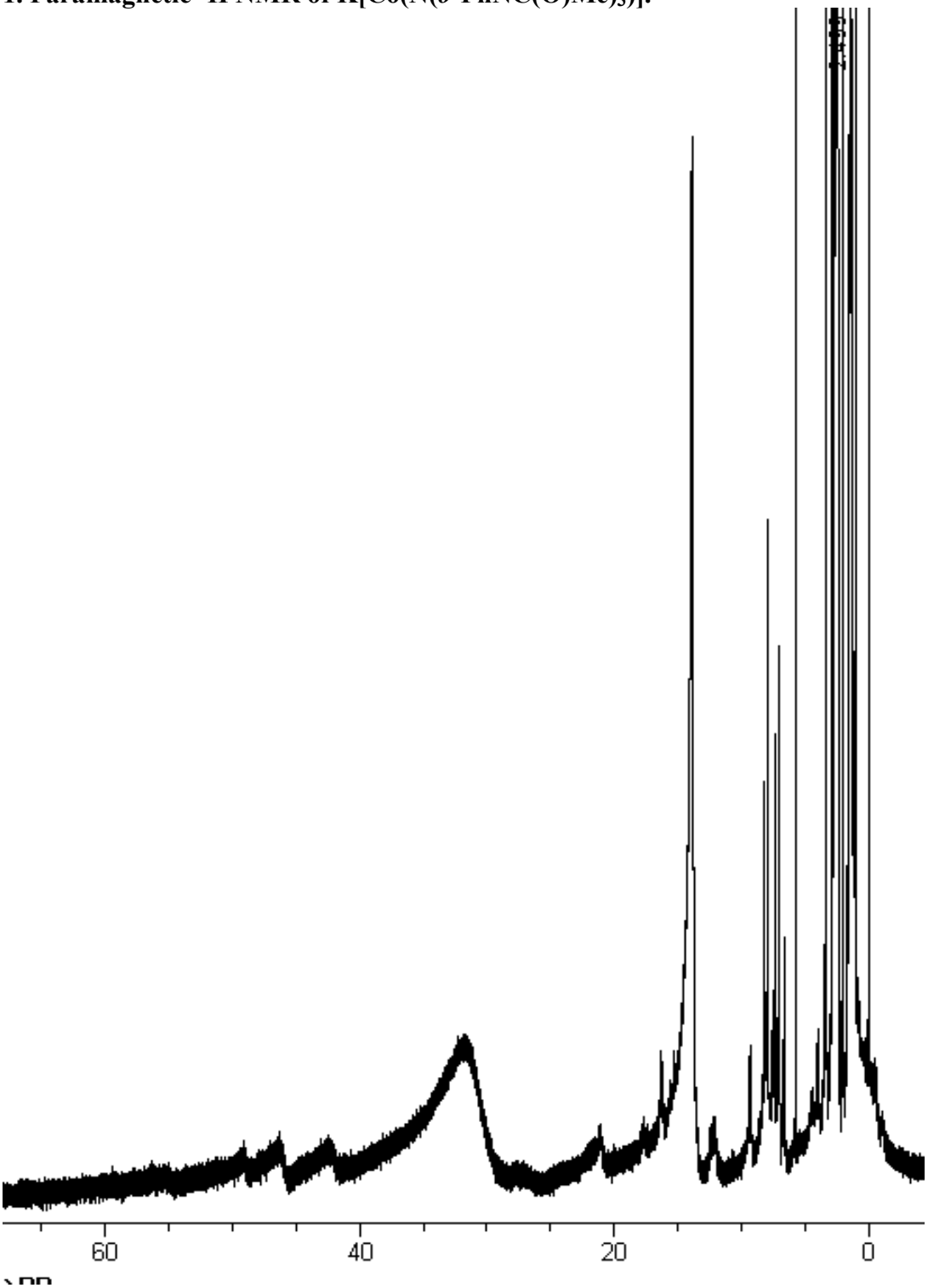

2. FTIR of K[Co(N(*o*-PhNC(O)Me)$_3$)].

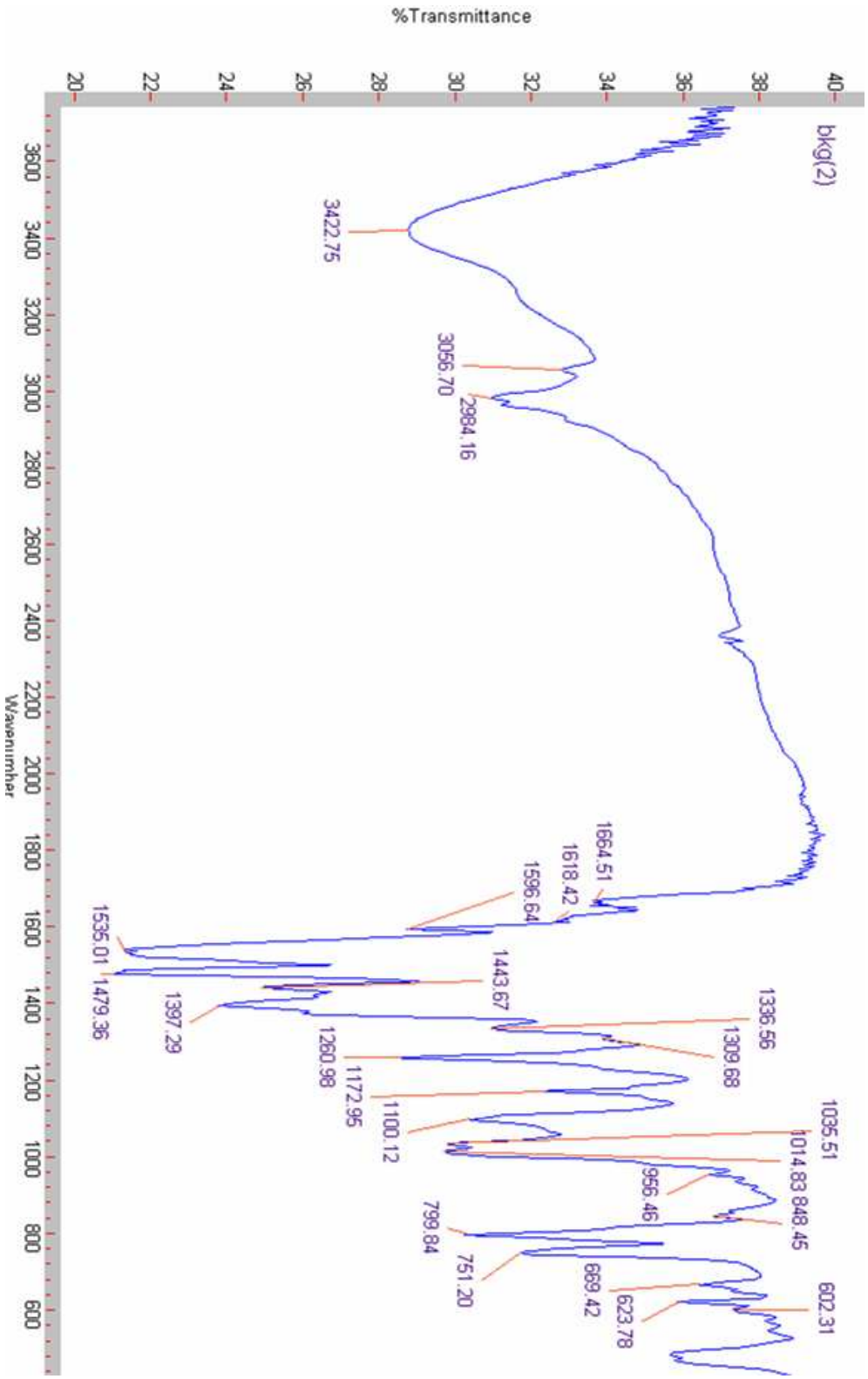

3. Electronic absorption spectrum of K[Co(N(*o*-PhNC(O)Me)$_3$)].

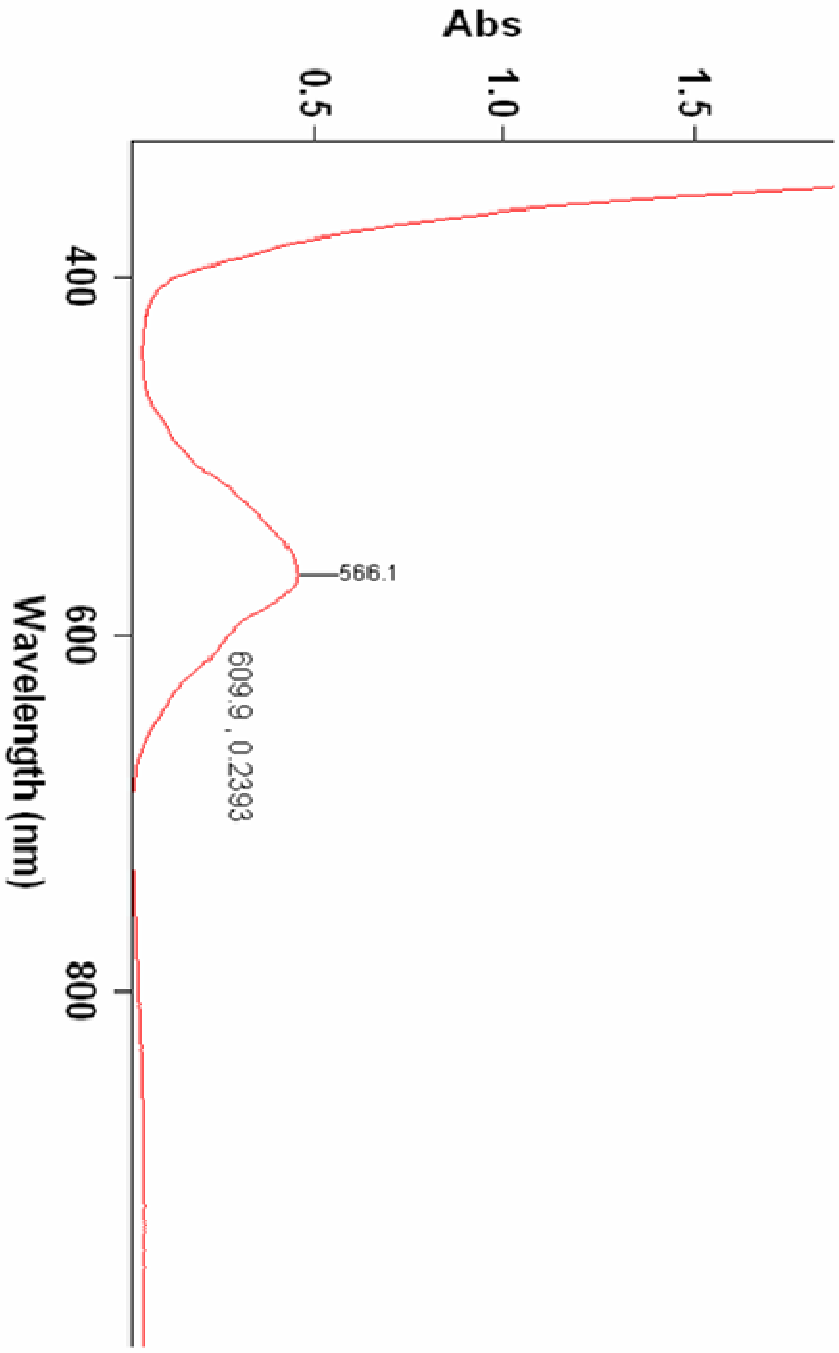

4. Negative ion ESI of K[Co(N(*o*-PhNC(O)Me)$_3$)].

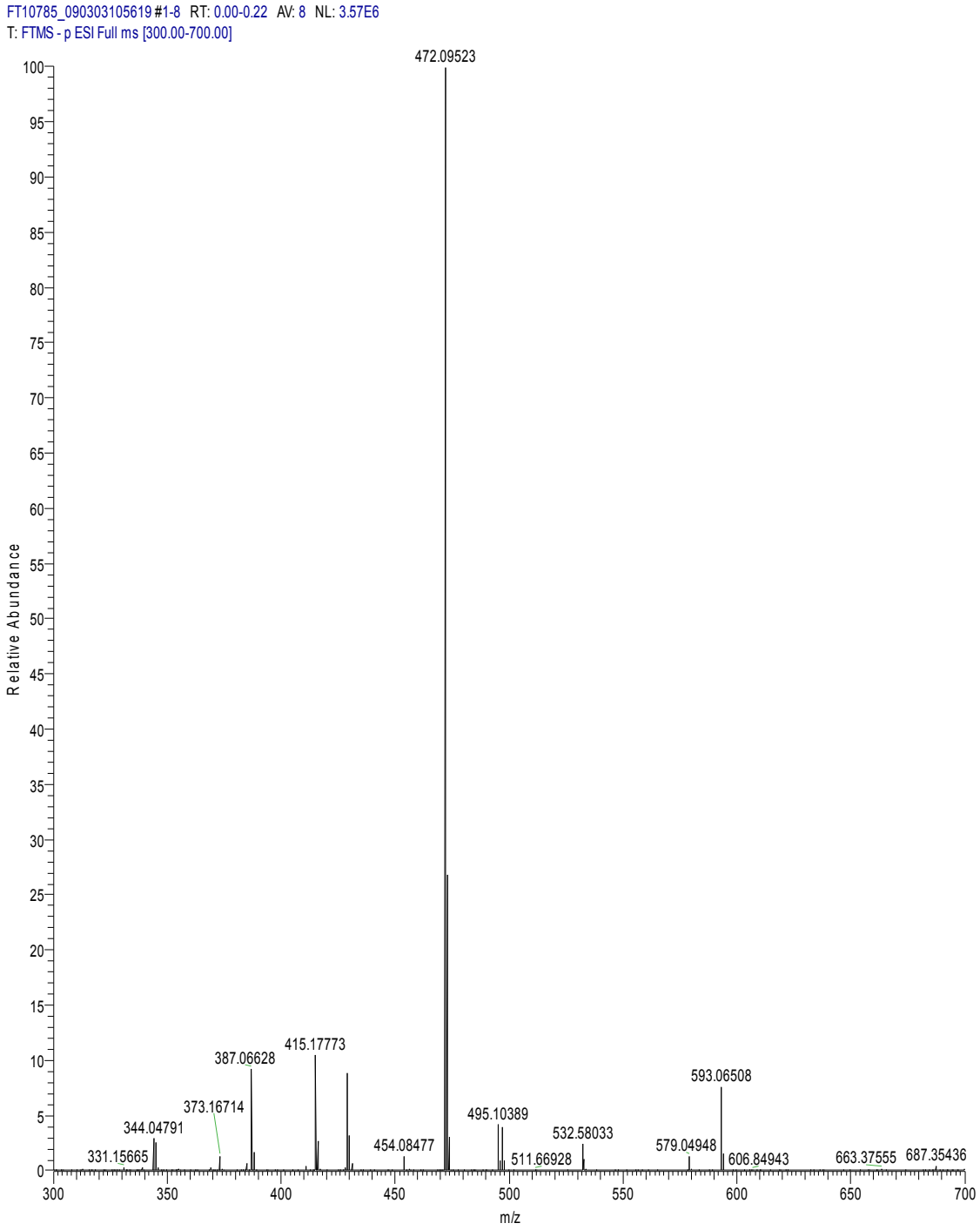

Appendix C. Spectroscopic Data on K[Ni(N(*o*-PhNC(O)Me)$_3$)].
1. Paramagnetic ^{1}H NMR of K[Ni(N(*o*-PhNC(O)Me)$_3$)].

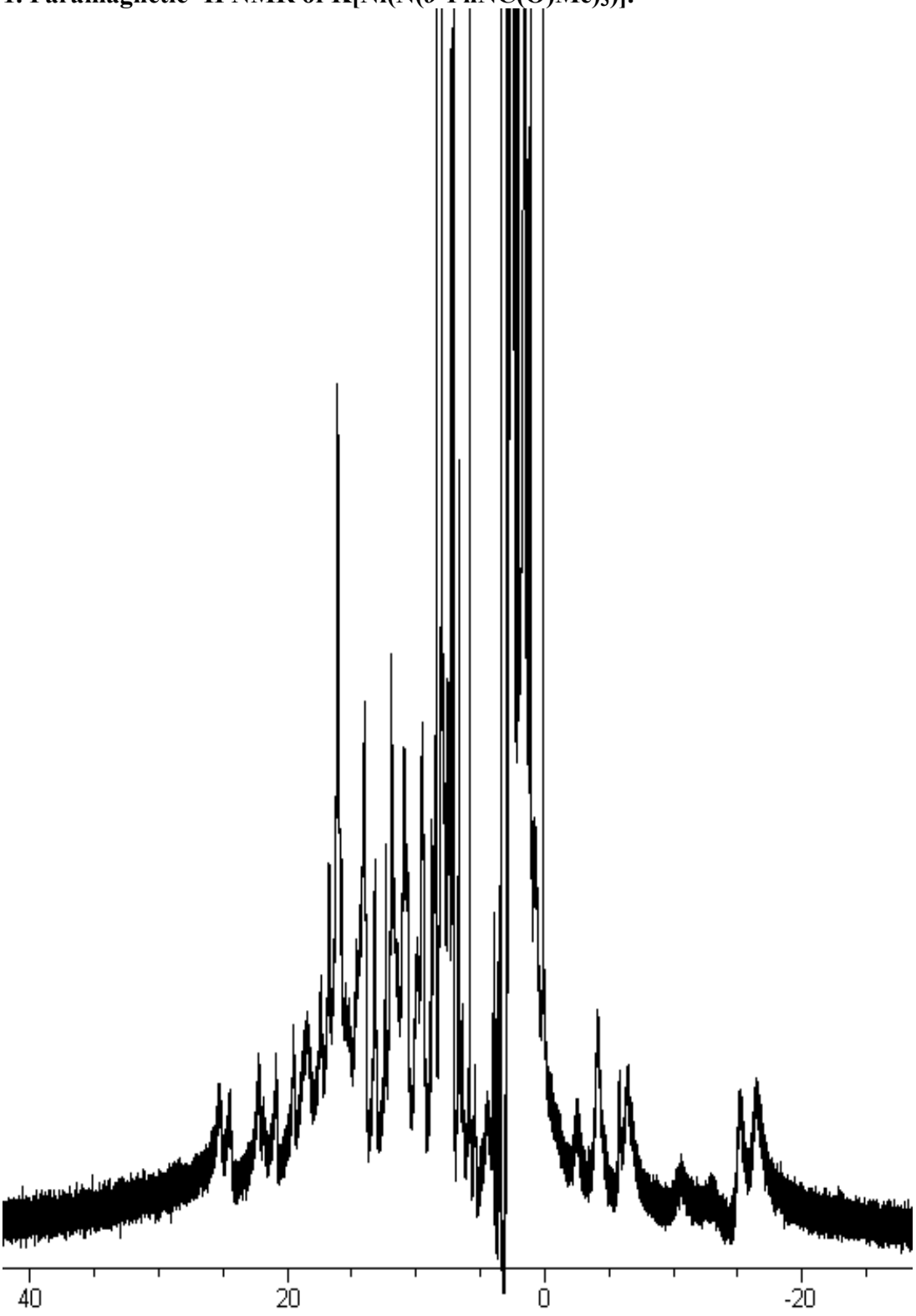

2. FTIR of K[Ni(N(*o*-PhNC(O)Me)$_3$)].

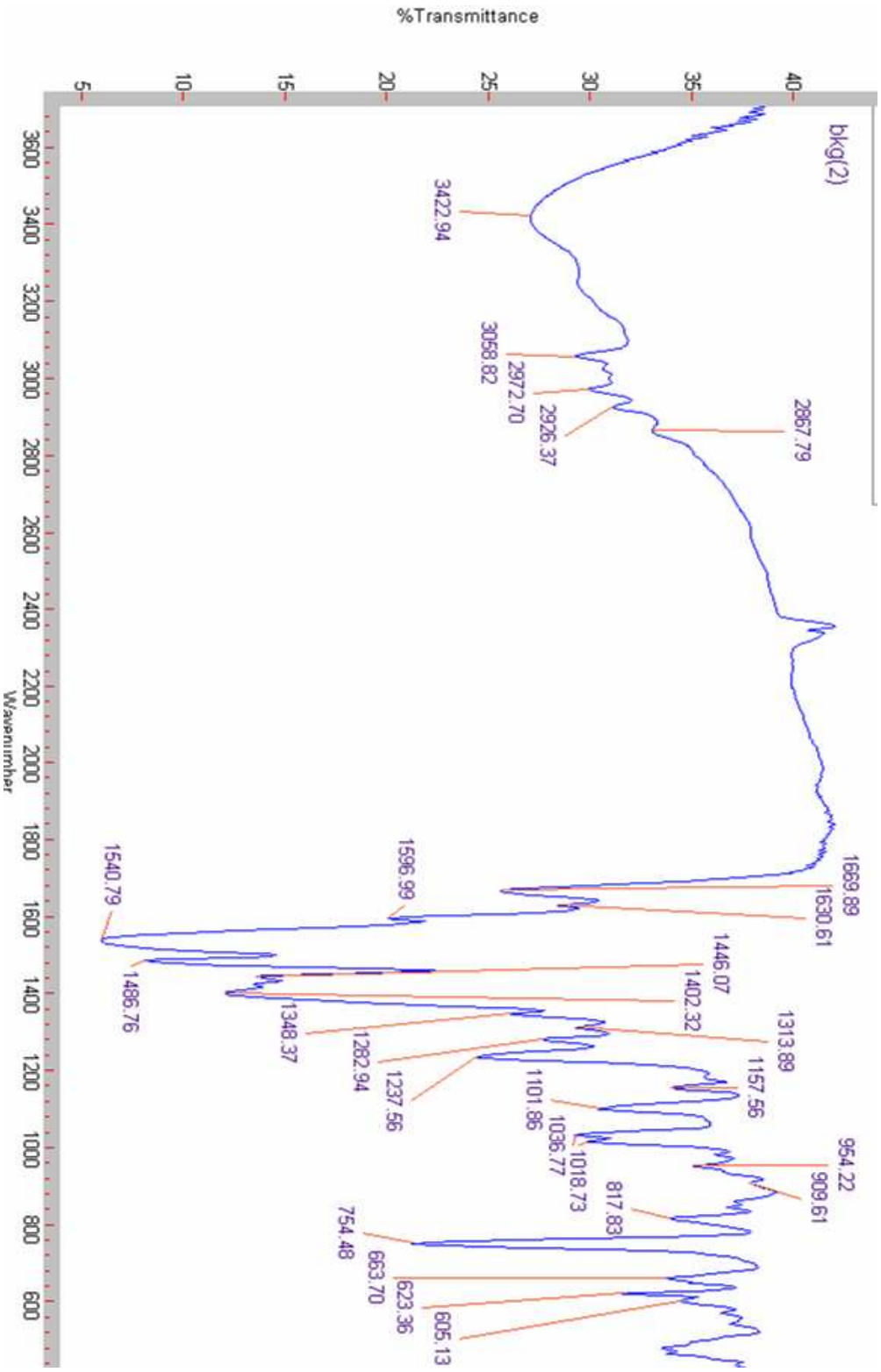

3. Electronic absorption of K[Ni(N(*o*-PhNC(O)Me)$_3$)].

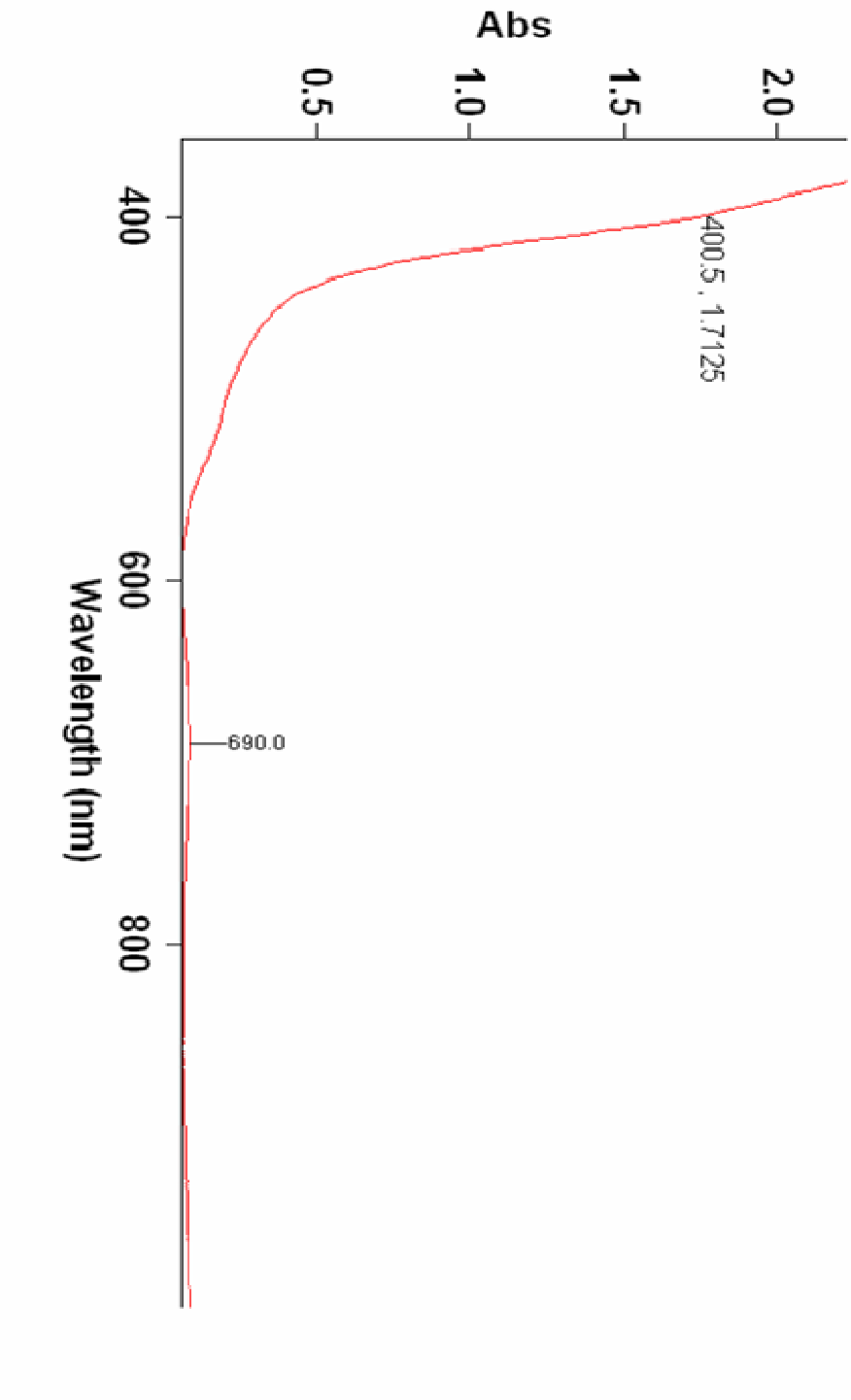

4. Negative ion ESI MS of K[Ni(N(*o*-PhNC(O)Me)$_3$)].

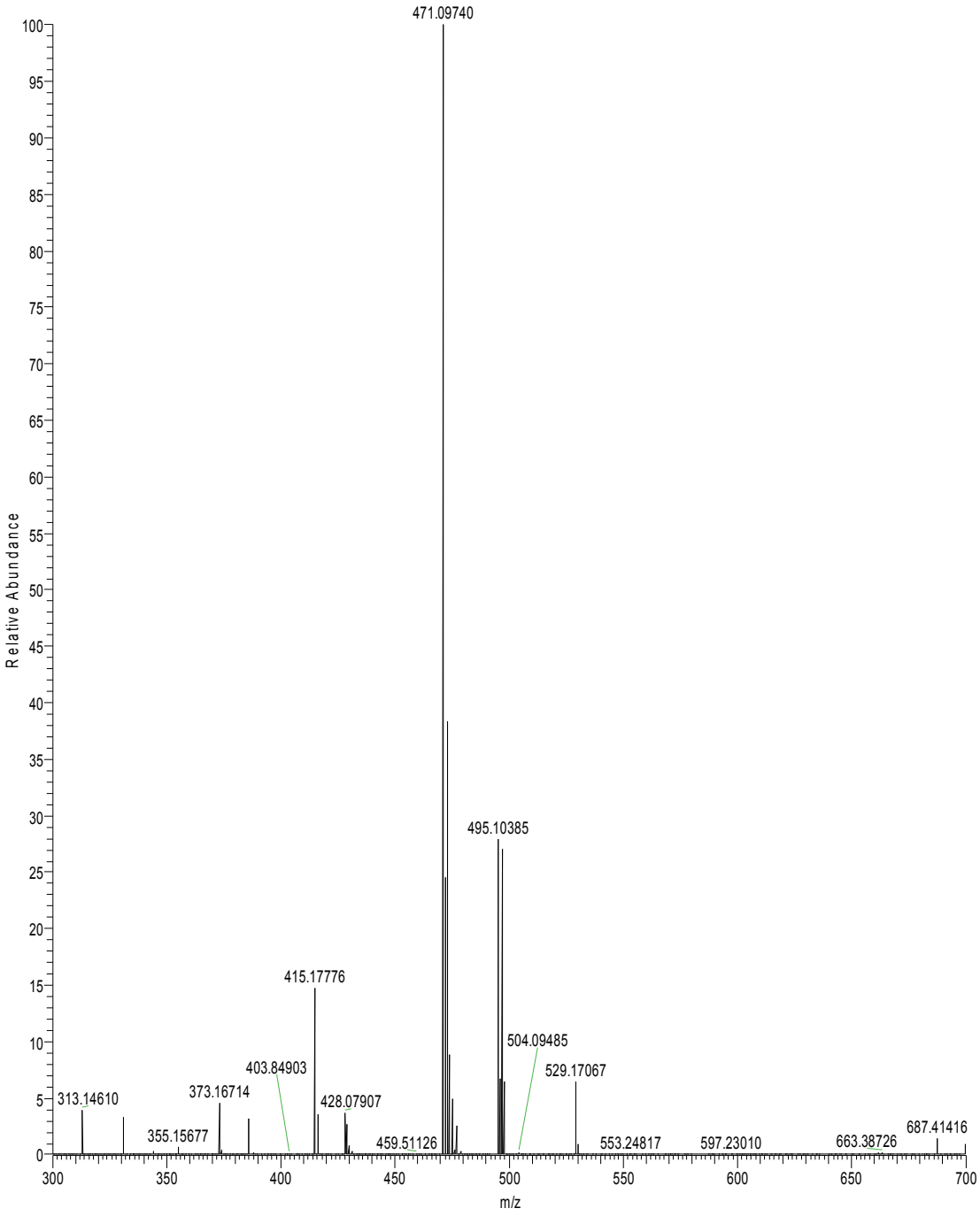

Appendix D. Spectroscopic Data on K[Zn(N(*o*-PhNC(O)Me)$_3$)].

1. ^{1}H NMR of K[Zn(N(*o*-PhNC(O)Me)$_3$)].

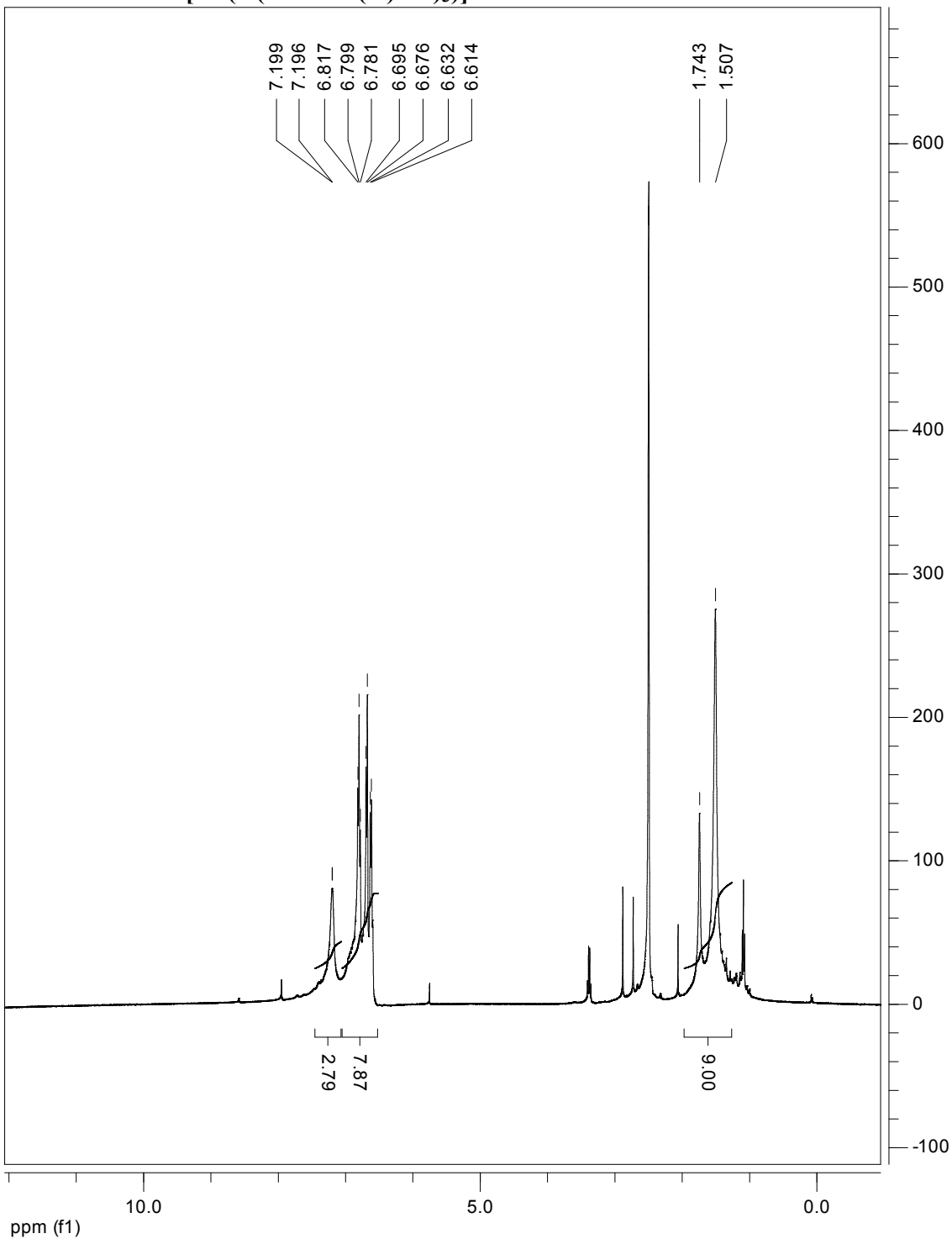

2. ^{13}C NMR of K[Zn(N(*o*-PhNC(O)Me)$_3$)].

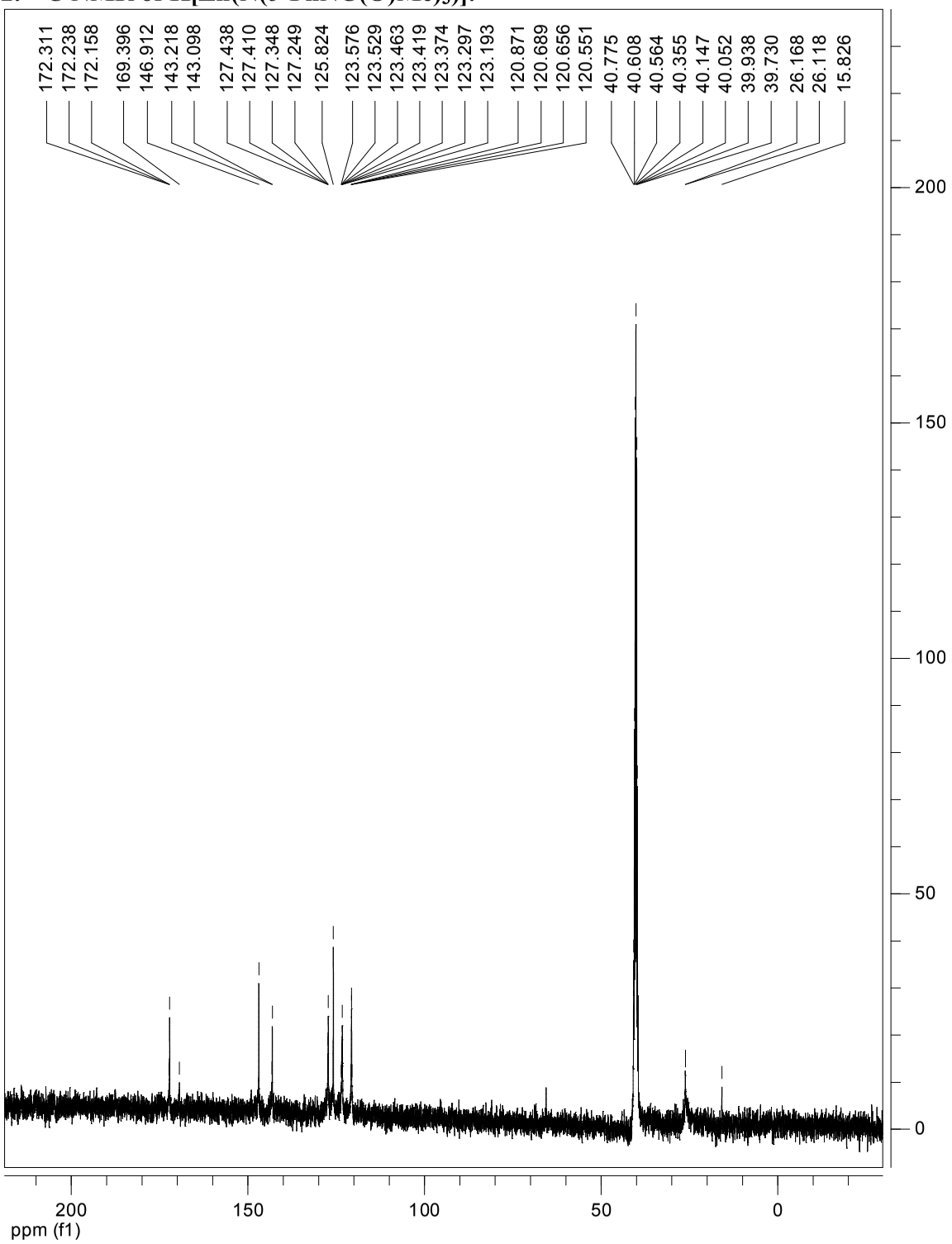

3. FTIR of K[Zn(N(*o*-PhNC(O)Me)$_3$)].

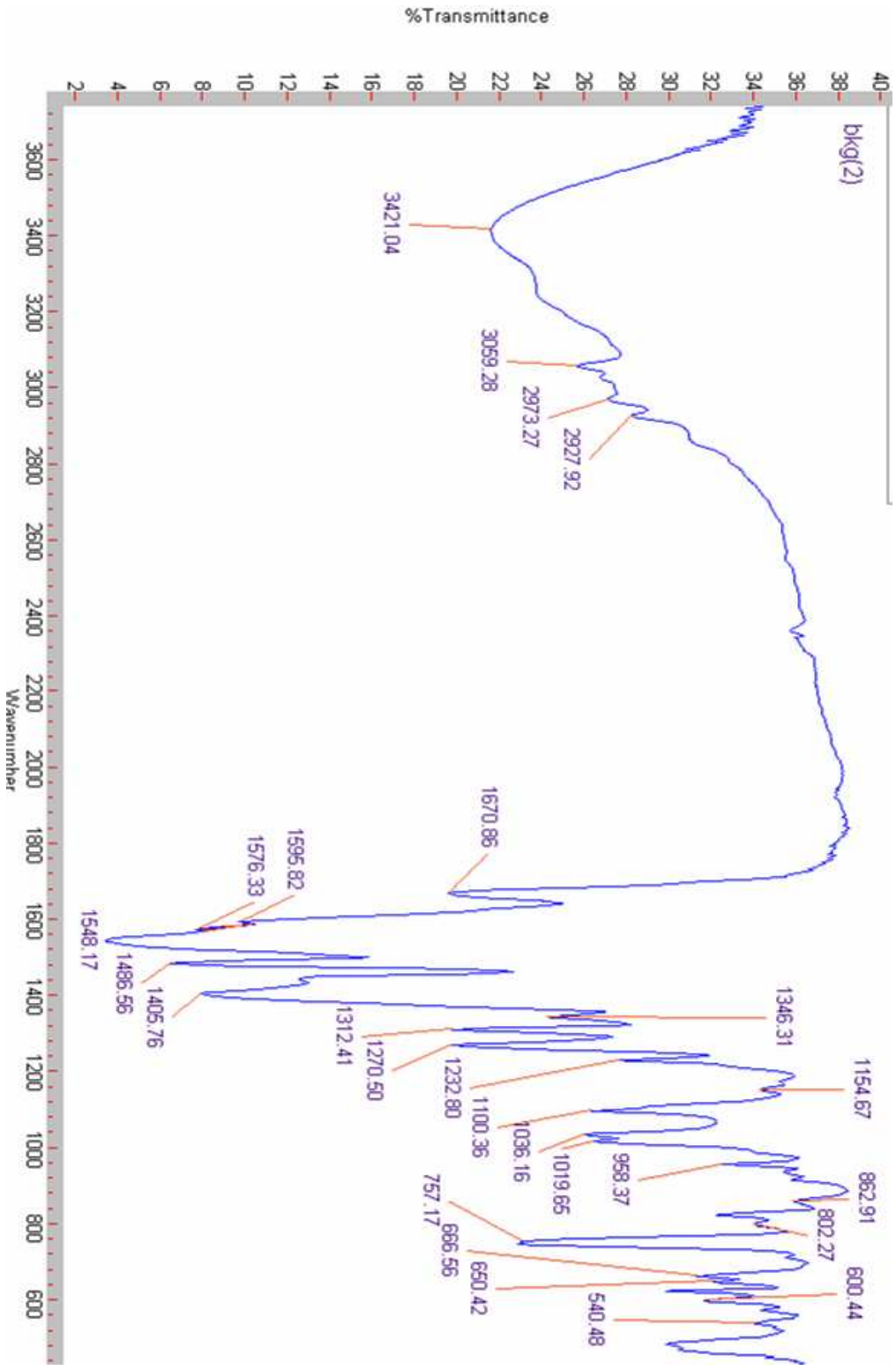

4. Negative ion ESI of K[Zn(N(*o*-PhNC(O)Me)$_3$)].

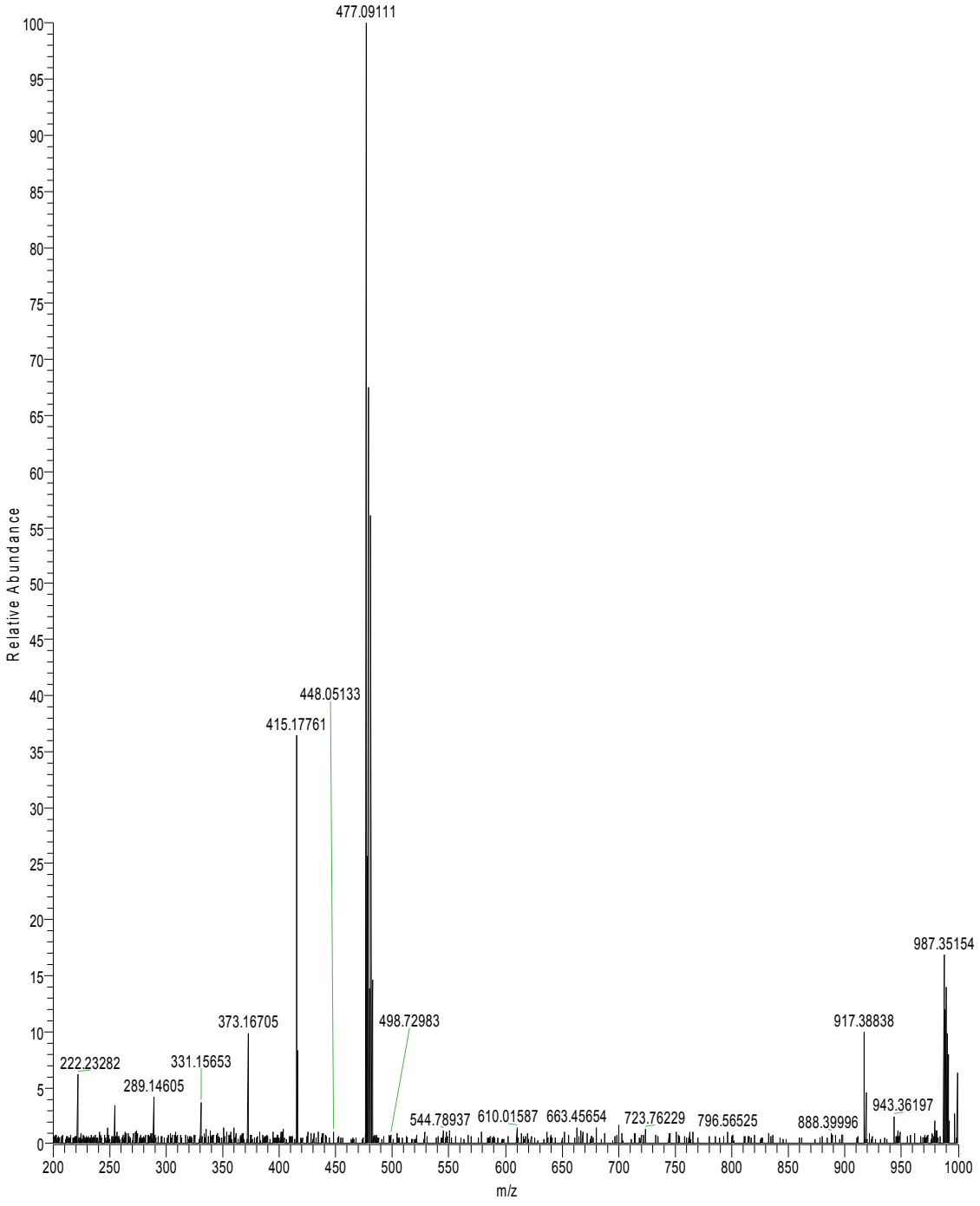

1 Blackman, A. G. *Polyhedron* **2005**, *24*, 1-39.
2 Jones, Matthew B. and Macbeth, C. E. *Inorg. Chem.* **2007**, *46*, 8117-8119.
3 Schrock, R. R. *Acc. Chem Res.* **1997**, *30*, 9-16.
4 Lee, Alison V and Schafer, Laurel L. *Eur. J. Inorg. Chem.* **2007**, 2243-2255.
5 (a) Fickes, M. G.; Davis, W. M.; Cummins, C. C. *J. Am Chem Soc.* **1995**, *117*, 6384. (b) Laplaza, C. E.; Davis, W. M.; Cummins, C. C. *Angew. Chem. Int. Ed. Engl.* **1995**, *34*, 2042. (c) Laplaza, C. E.; Cummins, C. C. *Science* **1995**, *268*, 861.,
6 (a) Memmler, H.; Gade, L. H.; Lauher, J. W. *Inorg. Chem.* **1994**, *33*, 3064. (b) Friedrich, S.; Memmler, H.; Gade, L. H.; Li, W.-S. *Angew. Chem. Int. Ed. Engl.* **1994**, *33*, 676. (c) Gade, L. H.; Becker, C.; Lauher, J. W. *Inorg. Chem*. **1993**, *32, 2308.*
7 (a) Cummins, C. C.; Lee, J.; Schrock, R. R.; Davis, W. M. *Angew. Chem. Int. Ed. Engl.* **1992**, *31, No. 11,* 1501-1503. (b) Pinkas, J.; Wang, T.; Jacobson, R. A.; Verkade, J. G. *Inorg. Chem.*, **1994**, *33*, 4202-4210. (c) Verkade, J. G. *Acc. Chem. Res.* **1993,** *26,* 483-489. (d) Roussel, P.; Alcock, N. W.; Scott, P. *Chem. Comm*. **1998**, *7*, 801-802. (e) Filippou, A. C.; Schneider, S.; Schnakenburg, G. *Inorg. Chem.* **2003**, *42*, 6974-6976.
8 (a) Mederos, A.; Dominguez, S.; Hernandez-Molina, R.; Sanchiz, J.; Brito, F. *Coord. Chem. Rev.* **1999**, *193-195*, 857-911. (b)Zanello, P. Metal Complexes Containing Redox Active Ligands. *Inorganic Electrochemistry: Theory, Practice, and Application*; Royal Society of Chemistry: Cambridge, UK, 2003; pp. 325-374.
9 Fleischer, E. B.; Gebala, A. E.; Tasker, P. A. *Inorg. Chim. Acta.* **1972**, *6*, 72-76.
10 Niemoth-Anderson, J. D.; Clark, K. A.; George, T. A.; Ross, C. R. *J. Am. Chem. Soc.* **2000**, *122*, 3977.
11 Mederos, A.; Dominguez, S.; Hernandez-Molina, R.; Sanchiz, J.; Brito, F. *Coord. Chem. Rev.* **1999**, *193*, 913-939.
12 (a) Frye, C. L.; Vincent, G. A; Hauschildt, G. L. *J. Am. Chem. Soc.* **1966**, *88*, 2727-2730. (b) Redshaw, C.; Rowan, M. A.; Homden, D. M.; Dale, S. H.; Elsegood, M. R. J.; Matsui, S.; Matsuura, S. *Chem. Comm.*, **2006**, 3329-3331. © Michalczyk, L.; de Gala, S.; Bruno, J. W. *Organometallics* **2001**, *21*, 5547-5556.
13 MacBeth, C. E.; Harkins, S. B.; Peters, J. C. *Can. J. Chem.*, **2005**, *83*, 332-340.
14 Although silylated derivatives such as [N(*o*-PhNHSiEt$_3$)$_3$] and [N(*o*-PhNHSiMe$_3$)$_3$] have been reported in their early transition metal complexes. See: Baumann, R. Group 4 Complexes Containing Tridentate Diamido Donor Ligands. Organometallic Chemistry and Catalysis, Ph.D. Thesis, Massachusetts Institute of Technology, Cambridge, MA, Feb. 1999.
15 Christou, V.; Arnold, J. *Angew. Chem. Int. Ed. Engl.* **1993***, 32*, 1450-1452.
16 Cummins, C. C.; Schrock, R. R.; Davis, W. M. *Angew. Chem. Int. Ed. Engl.* **1993**, *32*, 756.
17 Cummins, C. C.; Schrock, R. R.; Davis, W. M. *Organometallics* **1992**, *11*, 1452.
18 Cummins, C. C.; Schrock, R. R. *Inorg. Chem.*, **1994**, *33*, 395-396.
19 (a) Yandulov, D. V.; Schrock, R. R. *Science* **2003**, *301*, 76-78. (b) Ritleng, V.; Yandulov, D. V.; Weare, W. W.; Schrock, R. R.; Hock, A. S.; Davis, W. M. *J. Am. Chem. Soc.* **2004**, *126*, 6150-6163. (c) Chen, J.; Woo, L. K. *J. Organomet. Chem.* **2000**, *601*, 57-68.
20 Macbeth, C. E.; Gupta, R.; Mitchell-Koch, K. R.; Young, V. G., Jr.; Lushington, G. H.; Thompson, W. H.; Hendrich, M. P.; Borovik, A. S. *J. Am. Chem. Soc.* **2004**, *126*, 2556-2567.
21 Ray, M.; Hammes, B.; Yap, Glenn, P. A.; Rheingold, A. L.; Borovik, A. S. *Inorg. Chem.* **1998**, *37*, 1527-1532.
[22] Gorvin, J. H. *J. Chem. Soc., Perkin Trans. I* **1988**, *6*, 1331-1335.
[23] Jones, Matthew B. and Macbeth, C. E. *Inorg. Chem.* **2007**, *46*, No. 20, supporting information.
[24] Jones, Matthew B. and Macbeth, C. E. *Inorg. Chem.* **2007**, *46*, No. 20, supporting information.
[25] Tan, J. D., Hudson, S. E., Brown, S. J., Olmstead, M. M., Mascharak, P. K. *J. Am. Chem. Soc.* **1992**, *114*, 3841-3853.
[26] Bernhardt, P. V., Mattsson, J., Richardson, D. R. *Inorg. Chem.* **2006**, *45*, 752-760.
[27] (a) Cabaleiro, S., Castro, J., Garcia-Vazquez, J. A., Romero, J., Sousa, A. *Polyhedron* **2000**, *19*, 1607-1614. (b) Rheingold, A. L., Liable-Sands, L. M., Golen, J. A., Yap, Glenn P. A., Trofimenko, S. *Dalton Trans.* **2004**, 598-604 (c) Rheingold, A. L., Incarvito, C. D., Trofimenko, S. *Inorg. Chem.* **2000**, *39,*

5569-5571.

[28] Belokon, Y. N., et al. *J. Am. Chem. Soc.* **2003**, *125*, 12860-12871.

[29] (a) Rheingold, A. L., Liable-Sands, L. M., Golen, J. A., Yap, Glenn P. A., Trofimenko, S. *Dalton Trans.* **2004**, 598-604. (b) Meyer, F., Jacobi, A., Nuber, B., Rutsch, P., Zsolnai, L. *Inorg. Chem.* **1998**, *37*, 1213-1218. (c) Yonemura, M., Arimura, K., Inoue, K., Usuki, N, Ohba, M., Kawa, H. *Inorg. Chem.* **2002**, *41*, 582-589.

[30] Bernhardt, P. V., Mattsson, J., Richardson, D. R. *Inorg. Chem.* **2006**, *45*, 752-760.

[31] Latos-Grayski, L., Johnson, J., Attar, S., Olmstead, M. M., Balch A. L. *Inorg. Chem.* **1998**, *37*, 4493-4499.

[32] Bernhardt, P. V., Mattsson, J., Richardson, D. R. *Inorg. Chem.* **2006**, *45*, 752-760.

[33] (a) Rheingold, A. L., Incarvito, C. D., Trofimenko, S. *Inorg. Chem.* **2000**, *39,* 5569-5571. (b) Yonemura, M., Arimura, K., Inoue, K., Usuki, N, Ohba, M., Kawa, H. *Inorg. Chem.* **2002**, *41*, 582-589. (c) Roy, M., Pathak, B., Patra, A. K., Jemmis, E. D., Nethaji, M., Chakravarty, A. R. *Inorg. Chem.* **2007**, *46*, 11122-11132.